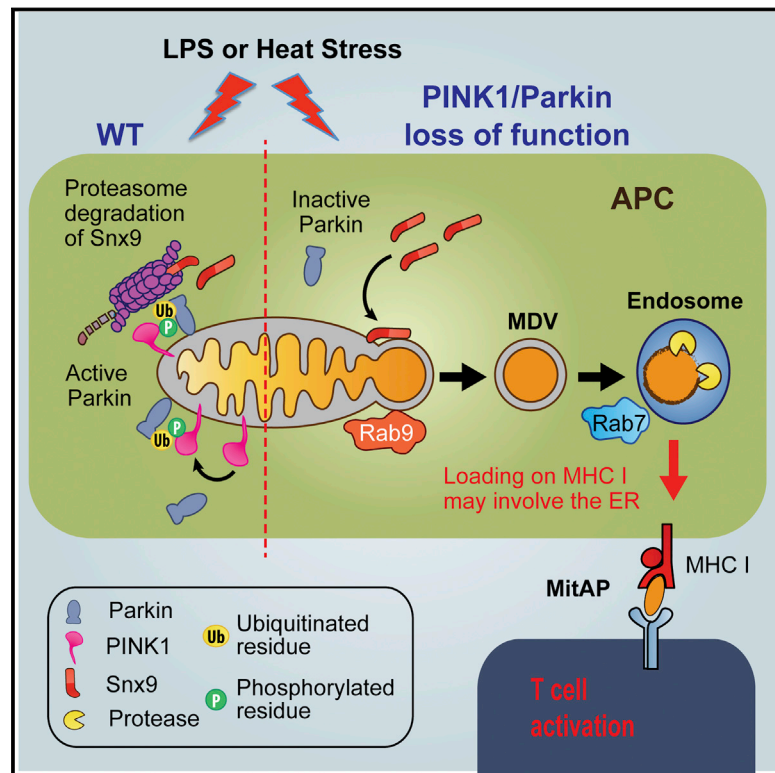


Parkinson's Disease-Related Proteins PINK1 and Parkin Repress Mitochondrial Antigen Presentation

Graphical Abstract



Authors

Diana Matheoud, Ayumu Sugiura, Angélique Bellemare-Pelletier, ..., Etienne Gagnon, Heidi M. McBride, Michel Desjardins

Correspondence

heidi.mcbride@mcgill.ca (H.M.M.), michel.desjardins@umontreal.ca (M.D.)

In Brief

PINK and PARKIN, two proteins that have been linked to Parkinson's disease, suppress antigen presentation from the mitochondria in immune cells, raising an autoimmune hypothesis for how mutations in these proteins cause neurodegeneration.

Highlights

- Parkinson's disease proteins PINK1 and Parkin regulate adaptive immunity
- PINK1 and Parkin inhibit mitochondrial antigen presentation (MitAP) in vitro and in vivo
- MitAP is driven by mitochondria-derived vesicles, not by mitophagy
- Autoimmune mechanisms are likely involved in Parkinson's disease

Parkinson's Disease-Related Proteins PINK1 and Parkin Repress Mitochondrial Antigen Presentation

Diana Matheoud,¹ Ayumu Sugiura,² Angélique Bellemare-Pelletier,¹ Annie Laplante,¹ Christiane Rondeau,¹ Magali Chemali,¹ Ali Fazel,³ John J. Bergeron,³ Louis-Eric Trudeau,⁴ Yan Burelle,⁵ Etienne Gagnon,⁶ Heidi M. McBride,^{2,7,*} and Michel Desjardins^{1,7,*}

¹Département de Pathologie et Biologie Cellulaire, Université de Montréal, C.P. 6128, Succursale centre-ville, Montréal, QC H3C 3J7, Canada

²Montreal Neurological Institute, McGill University, 3801 University Avenue, Montreal, QC H3A 2B4, Canada

³Department of Medicine, McGill University Hospital Research Institute, Montreal, QC H4A 3J1, Canada,

⁴Departments of Pharmacology and Neurosciences, Université de Montréal, Montreal, QC H3C 3J7, Canada

⁵Faculty of Pharmacy, Université de Montréal, Montréal, QC H3C 3J7, Canada

⁶Institute for Research in Immunology and Cancer and Department of Immunology, Université de Montréal, Montréal, QC H3C 3J7, Canada

⁷Co-senior author

*Correspondence: heidi.mcbride@mcgill.ca (H.M.M.), michel.desjardins@umontreal.ca (M.D.)

<http://dx.doi.org/10.1016/j.cell.2016.05.039>

SUMMARY

Antigen presentation is essential for establishing immune tolerance and for immune responses against infectious disease and cancer. Although antigen presentation can be mediated by autophagy, here we demonstrate a pathway for mitochondrial antigen presentation (MitAP) that relies on the generation and trafficking of mitochondrial-derived vesicles (MDVs) rather than on autophagy/mitophagy. We find that PINK1 and Parkin, two mitochondrial proteins linked to Parkinson's disease (PD), actively inhibit MDV formation and MitAP. In absence of PINK1 or Parkin, inflammatory conditions trigger MitAP in immune cells, both in vitro and in vivo. MitAP and the formation of MDVs require Rab9 and Sorting nexin 9, whose recruitment to mitochondria is inhibited by Parkin. The identification of PINK1 and Parkin as suppressors of an immune-response-eliciting pathway provoked by inflammation suggests new insights into PD pathology.

INTRODUCTION

Antigen presentation is a complex proteolytic process enabling cells to display antigens on their surface, informing the immune system about a cell's physiological status. These antigens allow T cells to distinguish normal cells from aberrant forms generated during diseases, including a wide range of infectious diseases and cancer (Guermónprez et al., 2002). Two classical pathways of antigen presentation have been described for the presentation of endogenous proteins on MHC class I molecules, and the presentation of exogenous antigens, such as intracellular pathogens, on MHC class II molecules (Blum et al., 2013). While the MHC II pathway is performed by specialized cells, such as macrophages and dendritic cells, virtually all cell types present pep-

tides on MHC I molecules, ensuring efficient monitoring of the organism by the immune system. It has been shown recently that autophagy, the recycling of self-components through lysosomal degradation, is involved in the presentation of endogenous antigens on both MHC class I and class II molecules (Englisch et al., 2009; Paludan et al., 2005), highlighting that vacuolar content also can be presented on MHC class I molecules.

In the thymus, sampling cellular antigens through autophagy plays a role in establishing immune tolerance (Nedjic et al., 2008), a process essential to limiting the occurrence of autoimmune diseases. Thus, understanding the pathways by which components from various organelles are sampled for presentation is of prime importance. In this context, little is known about the mechanisms regulating the presentation of mitochondria antigens, despite that this organelle is associated with the autoimmune disease primary biliary cirrhosis (PBC) (Hirschfield and Gershwin, 2013). Considering the involvement of autophagy in antigen presentation, one would assume that mitophagy, the selective process by which mitochondria are captured for degradation (Eiyama and Okamoto, 2015), would actively participate in mitochondrial antigen presentation (MitAP). Such a process would influence a disease like Parkinson's disease (PD), since mutations in genes coding for two proteins involved in mitophagy, PINK1 and Parkin, are responsible for the early onset recessive form of PD (Hernandez et al., 2016).

PINK1 and Parkin regulate mitophagy and reactive oxygen species (ROS)-induced mitochondrial-derived vesicle (MDV) transport to late endosomes (McLelland et al., 2014; Pickrell and Youle, 2015). In this context, the current model of PD proposes that defects in PINK1 and Parkin cause an accumulation of dysfunctional mitochondria, leading to the loss of DA neurons with age (Pickrell and Youle, 2015). Indeed, PINK1 is a kinase stabilized at the surface of damaged mitochondria, where it phosphorylates both ubiquitin and Parkin, promoting the recruitment of mitophagy receptors (Heo et al., 2015; Lazarou et al., 2015). However, several observations point to a significant contribution of the immune system in the etiology of PD. These include microglial activation, an increase in the expression of

inflammatory genes, local inflammation, and infiltration of immune cells in the brain of PD patients (Kannarkat et al., 2013; Mosley et al., 2012). Recent studies have shown that DA neurons express MHC class I molecules at their surface in the presence of activated microglia and inflammation (Cebrián et al., 2014) and that mice lacking MHC II are protected against MPTP-induced degeneration (Martin et al., 2016), providing further support for the plausibility of the contribution of immune mechanisms in the development of PD. These observations led us to investigate the role of mitophagy in antigen presentation and whether PINK1 and/or Parkin may influence this process.

Here, we present *in vitro* and *in vivo* data demonstrating that PINK1 and Parkin play an active role in the repression of MitAP. In the absence of these proteins, high levels of mitochondrial antigens are presented on MHC class I molecules in both macrophages and dendritic cells by a vacuolar pathway distinct from mitophagy. Presentation of mitochondrial antigens is driven instead by the formation of mitochondria-derived vesicles (MDVs), a quality control mechanism allowing the shuttle of specific mitochondrial cargos to late endosomes (Sugiura et al., 2014). We have found that both MDV formation and MitAP require Sorting nexin 9 (Snx9), a dynamin-binding partner essential for clathrin-mediated endocytosis (Lundmark and Carlsson, 2009). The recruitment of this protein to mitochondria is actively inhibited by Parkin. Rab9, a late endosomal/Golgi guanosine triphosphatase (GTPase) that regulates vesicle release from late endosomes (Kucera et al., 2015), is also recruited to mitochondria for the formation of MDVs, while a second GTPase, Rab7, regulates the fusion of MDVs with endosomal compartments. These data identify an antigen presentation pathway regulated by PINK1 and Parkin, providing a link between mitochondrial dynamics and the potential engagement of autoimmune mechanisms in the etiology of PD.

RESULTS

A Mitochondrial Reporter Antigen Is Presented by a Vacuolar Pathway

To test whether mitophagy is responsible for the presentation of mitochondrial antigens, we developed a system in which the glycoprotein B (gB) of herpes simplex virus 1 (HSV1) is expressed in a murine macrophage cell line (RAW) and targeted to the mitochondrial matrix (mito-gB). As controls, RAW cells expressing gB targeted to either the nuclear envelope (NE-gB) or the cytoplasm (cyto-gB) (Figure 1A) were also produced. This approach allowed us to use a gB-specific CD8⁺ T cell hybridoma recognizing the gB_{498–505} peptide loaded on MHC class I molecules to monitor antigen presentation (Mueller et al., 2002). In steady-state conditions (37°C), the presentation of mito-gB, unlike the other two forms of gB, was dependent on vacuolar processing (Figure 1B). This is shown by the partial inhibition of mito-gB presentation in cells in which the vacuolar proton pump is inhibited with bafilomycin A (Baf) and by the increase in cells treated with a cocktail of lysosomal proteases inhibitors (PI), a condition that slows the complete degradation of proteins into amino acids within endocytic compartments (English et al., 2009). The presentation of mito-gB also distinguished itself by being insensitive to cycloheximide treatment (Figure 1C; raw

values in Figure S1A), indicating that gB localized in the mitochondria matrix is presented, rather than newly synthesized cytosolic precursor forms. To further exclude the possibility that mito-gB mistargeted to the cytoplasm is presented, we treated cells with IFN γ to stimulate the classical proteasome pathway of antigen presentation (Trost et al., 2009). In these conditions, cyto-gB and NE-gB (exposed on the cytoplasmic side of the nuclear membrane) were efficiently presented (Figure 1D) in a Baf-insensitive way (Figure 1E). As expected, treatment with the proteasome inhibitor MG132 strongly inhibited presentation. In contrast, IFN γ had no effect on the presentation of mito-gB, ruling out the cytoplasm as a source of antigen. To further demonstrate that mito-gB was processed through a vacuolar pathway, we treated cells with a short, 45-min heat stress (HS), a condition known to stimulate autophagy (Nivon et al., 2009) and the vacuolar processing of endogenous proteins (Trost et al., 2009). In these conditions, mito-gB presentation was increased by more than 20-fold (Figure 1D; raw values in Figure S1B). Importantly, on return to 37°C, mitochondria remained fully functional with equivalent maximal respiratory rates, no increase in ROS production, or no loss in mitochondrial mass (Figures S1C–S1F). This ruled out a sustained toxic effect of the HS on mitochondria. The presentation of the two other forms of gB was also enhanced (Figure 1D) in a Baf-sensitive way (Figure 1E).

Mitophagy Is Not Responsible for Mitochondrial Antigen Presentation

We then examined whether the presentation pathway(s) induced during HS were related to autophagy/mitophagy. We treated cells with 3-methyladenine (3-MA) or downregulated the expression of ATG5 by small hairpin RNA (shRNA) (using a scramble shRNA as control), two robust methods to inhibit autophagy and mitophagy (Liu et al., 2012; Narendra et al., 2008). Efficiency of knockdown (KD) was confirmed by qPCR (Table 1). These conditions inhibited the presentation of NE-gB and cyto-gB during HS, confirming the involvement of autophagy in their capture (Figure 2A). Remarkably, mito-gB presentation was stimulated, not inhibited, indicating that mitophagy, an ATG5-dependent pathway (Narendra et al., 2008), is not involved in MitAP, but, in fact, represses this process. To determine more precisely whether mitophagy plays a role in mito-gB presentation, we downregulated the expression of PINK1 by shRNA, a kinase required for mitophagy (Pickrell and Youle, 2015). In these conditions, mito-gB presentation was strongly enhanced (Figure 2B), while the presentation of NE-gB and cyto-gB was not altered (Figure 2C). We were unable to generate Parkin KD cells, possibly due to the low level of Parkin expression in RAW cells (Figure S2A). Therefore, we performed inverse experiments and observed that a mild expression of GFP-Parkin in RAW cells abolished mito-gB presentation on HS (Figure 2D), while it had no effect on the presentation of NE-gB (data not shown). These results indicate that PINK1 and Parkin specifically regulate MitAP.

Additional experiments ruled out the contribution of mitophagy in mito-gB presentation. We showed that mito-gB presentation was unaffected in cells silenced for the GTPase dynamin related protein 1 (Drp1) (Figure 2E), a protein required for mitochondria fragmentation and mitophagy (Narendra et al., 2008).

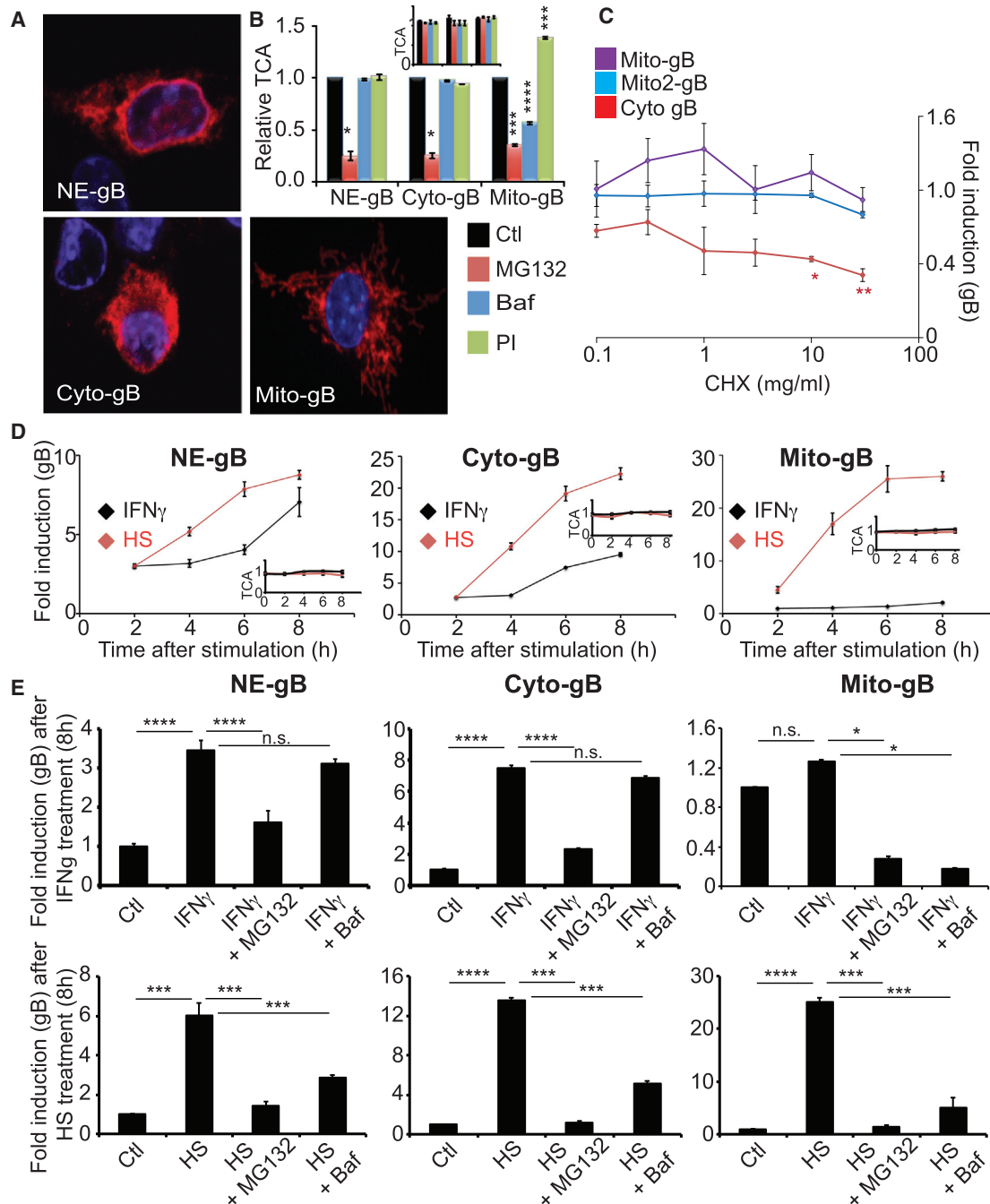


Figure 1. Mitochondrial Reporter Antigen Is Presented in a Vacuolar Pathway

(A) The glycoprotein B (gB) of herpes virus simplex 1 is expressed and targeted to the nuclear envelope/ER membrane (NE-gB), the cytoplasm (cyto-gB), or the mitochondrial matrix (mito-gB) of RAW 264.7 macrophages engineered to express the K^b MHC I allele. DAPI staining in blue shows the nucleus.

(B) Effect of the proteasome inhibitor MG132, the vacuolar proton pump inhibitor bafilomycin (Baf), and a cocktail of protease inhibitors on the presentation of the various gB constructs to the MHC class I-restricted 2E2 hybridoma. Inset shows the control peptide.

(C) Effect of CHX in mito-gB, mito-gB2 (a cell expressing a higher level of the protein), and cyto-gB MHC I presentation (see also Figure S1A).

(D) Effect of interferon- γ (IFN γ) and a 45-min 42°C heat stress (HS) on the presentation of gB. Insets show control peptide (see also Figure S1B).

(E) Effect of MG132 and Baf treatment on the presentation of gB following IFN γ or HS treatment. Data represent mean \pm SD of one experiment, representative of at least three independent experiments. p value is calculated using one (B and D) or two-way (C) ANOVA analyses.

See also Figure S1.

Table 1. Quantitative Measurement of shRNA Knockdown Efficiency by qRT-PCR

Atg5				
Sample Name	Target Name	RQ	RQ Min.	RQ Max.
Raw-mito-Scr	2-IR3947	1.000	0.894	1.119
Raw-mito-Atg5	2-IR3947	0.229	0.732	1.043
Raw-cyto-Scr	2-IR3947	1.000	0.872	1.146
Raw-cyto-Atg5	2-IR3947	0.209	0.185	0.237
Raw-NE-Scr	2-IR3947	1.000	0.795	1.258
Raw-NE-Atg5	2-IR3947	0.223	0.177	0.281
Drp1				
Sample Name	Target Name	RQ	RQ Min	RQ Max
Raw-mito-Scr	IR4715	1.000	0.860	1.163
Raw-mito Dnm1L-4	IR4715	0.415	0.349	0.492
Pink1				
Sample Name	Target Name	RQ	RQ Min	RQ Max
Raw-mito-Scr	1-IR3568	1.000	0.759	1.317
Raw-mito-Pink3	1-IR3568	0.409	0.338	0.494
Raw-cyto-scr	01-IR3568	1.000	0.920	1.087
Raw-cyto Pink1-3	01-IR3568	0.491	0.453	0.532
03-Raw-NE-scr	01-IR3568	1.000	0.851	1.175
04-Raw-NE Pink1-3	01-IR3568	0.407	0.369	0.449
Rab7				
Sample Name	Target Name	RQ	RQ Min	RQ Max
Raw-NE-Scr	IR4874	1.000	0.882	1.134
Raw-full-Rab7-4	IR4874	0.396	0.341	0.459
Snx9				
Sample Name	Target Name	RQ	RQ Min	RQ Max
Raw-mito-Scr	IR4585	1.000	0.805	1.242
Raw-mito_Snx9-3	IR4585	0.539	0.467	0.623
Raw-NE-Scr	IR4585	1.000	0.903	1.107
Raw-NE-Snx-9-3	IR4585	0.334	0.294	0.379

Efficiency of the Drp1 KD was confirmed by showing that mitochondria could no longer be fragmented by protonophore *m*-chlorophenylhydrazine (CCCP) treatment (Figure S2B). Furthermore, treatment with CCCP to maximally activate mitophagy had no effect on mito-gB presentation (Figure 2F). Efficiency of the treatment was confirmed through the induction of LC3 expression and degradation of mitofusin1 (Figures 2G and S2C). Similar results were obtained in RAW cells expressing GFP-Parkin (data not shown). These data demonstrate that mitophagy provides an efficient pathway for the capture and degradation of dysfunctional mitochondria in a way that limits antigen presentation. In that respect, mitophagy differs from autophagic pathways, such as macroautophagy (Paludan et al., 2005) and NEDA (English et al., 2009). This might be due to the fact that mitochondria are of bacterial origin. Because the immune system is able to recognize and mount an efficient response against bacteria phylogenetically related to mitochondria, it might be beneficial to limit the exposure of mitochondrial antigens to the immune system (Baum, 1995).

Mitochondria-Derived Vesicles Are Involved in Mitochondrial Antigen Presentation

Having shown that mitophagy is not involved in MitAP, we performed experiments to determine the nature of the Baf-sensitive pathway responsible for mito-gB presentation during HS. We showed previously that selective delivery of mitochondrial content to late endosomes occurs through mitochondria-derived vesicles (MDVs) (Soubannier et al., 2012). MDVs differ from mitochondrial fragments through at least three distinct criteria: (1) only selected cargo is incorporated within vesicles, (2) they are formed in a Drp1-independent manner, and (3) ultrastructural analysis reveals a limited diameter of 80–150 nm containing a single outer membrane or a double membrane-bound structure that lack cristae (Sugiura et al., 2014). With these criteria in mind, we examined whether a PINK1/Parkin-independent MDV pathway may be responsible for the induction of MitAP observed during HS. Immunofluorescence analyses (IF) indicated that the colocalized signals for mito-gB and the mitochondrial marker Tom20 dissociated on HS, mito-gB being observed in small vesicular-like structures lacking Tom20 throughout the cell (Figure 3A). To test whether these structures reflected membrane-bound vesicles, we performed biochemical fractionation. In control cells kept at 37°C, gB and Tom20 co-fractionated in the denser parts of a sucrose gradient (Figure 3B). As observed by IF, HS induced the dissociation of both markers, shifting a significant part of gB to lower density fractions. HSP60, a second matrix protein, was not shifted to light fractions on HS, supporting the concept that cargo-selective mechanisms operate during MDV formation. Consistent with mito-gB being a MDV cargo, in HS-treated cells, gB was pelleted at 110,000 × *g* from a post-mitochondrial supernatant and was soluble in the presence of detergent (Figure 3C). Confocal images at higher magnification revealed the lateral segregation of gB along mitochondrial tubules stained for Tom20, consistent with the selective enrichment of gB into vesicular structures (Figure 3D). Electron microscopy (EM) showed the emergence of small, double membrane-bound vesicular profiles (between 80–120 nm in diameter) from mitochondria in HS conditions, while these structures were not observed in our samples at 37°C (Figure 3D). These experiments are consistent with mito-gB being a matrix cargo, selectively incorporated within vesicular structures derived from mitochondria in a Drp1-independent manner on HS treatment. Lastly, mito-gB+/Tom20– MDVs were observed close to LAMP1+ compartments on HS (Figure 3E), suggesting that they might be involved in the trafficking of gB to degradative organelles for antigen processing.

Formation of MDVs and Mitochondrial Antigen Presentation Are Regulated by Rab7, Rab9, and Snx9

Since the processing of mito-gB was vacuolar, we assumed that MDVs interacted with late endosomes/lysosomes. This led us to study the potential involvement of Rab7 and Rab9, two small GTPases known to regulate the functional properties of these organelles (Chavrier et al., 1990; Lombardi et al., 1993), in MitAP. Downregulation of either GTPase strongly inhibited mito-gB presentation, with no effect on NE-gB presentation (Figure 4A). Specificity of the KD for Rab9 was confirmed by western blot (WB), as well as with rescue experiments (Figures S3A and

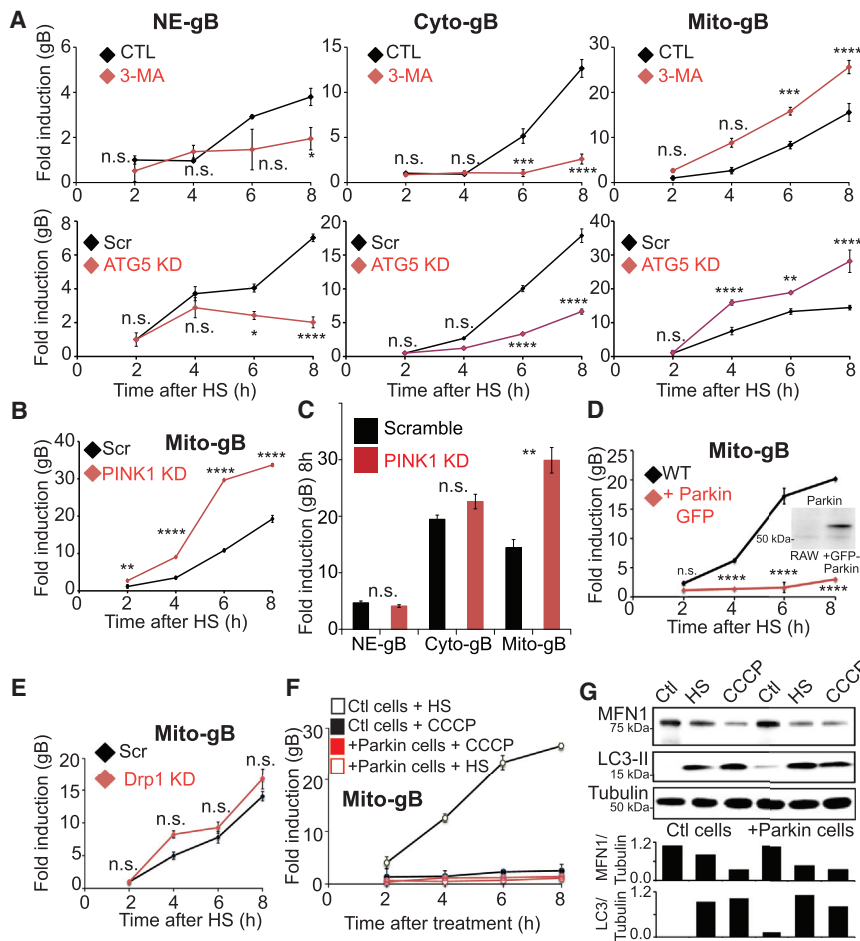


Figure 2. Mitophagy Is Not Responsible for MitAP

(A) Effect of the PI3K inhibitor 3-methyladenine (3-MA) or downregulation of ATG5 using shRNA (ATG5 KD) on gB presentation following HS. CTL, control cells in culture medium; Scr, cells transduced with scramble shRNA.

(B) Pink1 downregulation increases MitAP.

(C) PINK1 specifically regulates the presentation of mito-gB.

(D) Expression of Parkin-GFP in RAW cells inhibits MitAP. Inset shows western blot of Parkin expression in control cells and +Parkin-GFP cells.

(E) Drp1 downregulation had no effect on MitAP after HS.

(F) MitAP was poorly induced after CCCP treatment in control cells or in +Parkin-GFP cells (see also Figures S2B and S2C).

(G) Levels of LC3b and MFN1 were measured at different times after CCCP treatment by western blotting. Data represent mean \pm SD of one experiment, representative of at least three independent experiments. p value is calculated using two-way ANOVA analyses and Student's t test for (C). See also Figure S2.

S3B). IF showed that while mito-gB vesicles were efficiently generated and accumulated in the cytoplasm after HS in control and Rab7 KD cells, the formation of these vesicles was strongly inhibited in Rab9 KD cells (Figure 4B). On return to 37°C, mito-gB and Tom20 co-localized together in control cells (Figure 4C). This was not the case in Rab7 KD cells, suggesting that mito-gB vesicles were unable to release their content for processing in endocytic organelles. These results indicate that although both GTPases regulate the pathway of mito-gB presentation, they act at different steps of the process. Rab7 has been shown to be involved in membrane fusion between late endosomes and lysosomes (Vanlandingham and Ceresa, 2009), suggesting that this GTPase is either required for gB-vesicle fusion with late endosomes or that GTPase inhibition interferes with late endosome/lysosome maturation, preventing gB processing. That the presentation of NE-gB is not inhibited in Rab7 KD cells supports the former proposal. In contrast, the inhibition of mito-gB vesicle formation observed in Rab9 KD cells suggests that this small GTPase plays a role at an early step of the pathway, during vesicle formation/budding on mitochondria. This is supported by WB analyses showing that of the two GTPases, only Rab9 was recruited to mitochondria on HS (Figure 4D). Mitochondria analyzed in these experiments were devoid of major contaminants from endosomes or the Golgi apparatus (Figure S3C).

Since Rab9 plays a role in vesicle formation/budding of retrograde cargo from late endosomes (Dong et al., 2013), our data support the concept that Rab9 plays a similar role on mitochondria. Further experiments with RAW cells expressing constitutively inactive (S21N) or active (Q66L) Rab9 mutants confirmed that mito-gB vesicle formation (data not shown) and the presentation of this marker are regulated by the GTPase activity of Rab9 (Figure 4E). EM analyses showed the accumulation of small, double membrane-bound vesicles apparently unable to bud off mitochondria in Rab9 KD cells (Figure 4F), consistent with the IF results.

We also identified Snx9 as an essential component required for MDVs formation. Snx9 was picked from a genome-wide screen search for proteins affecting mitochondrial morphology (Norton et al., 2014) and considered interesting for the present study because of its established function in vesicle formation and intracellular membrane trafficking (Lundmark and Carlsson, 2009). To determine whether Snx9 played a role in mito-gB vesicle formation, we first tested the requirement for Snx9 in the established MDV transport pathway induced on oxidative stress (Soubannier et al., 2012). Confocal stacks confirmed the localization of YFP-Snx9 on mitochondria (Figure S4). Silencing Snx9 inhibited the formation of MDVs induced under oxidative stress (Figure S4B). Video microscopy showed that Snx9 transiently associated with mitochondria (Figure S4C), in foci that “flashed” on the membrane with an average duration of 24 s. These data suggest a role for Snx9 in the generation of oxidative-stress-induced MDVs. Downregulation of Snx9 in RAW cells strongly inhibited the formation of mito-gB vesicles (Figure 5A) and the presentation of this marker (Figure 5B). In contrast,

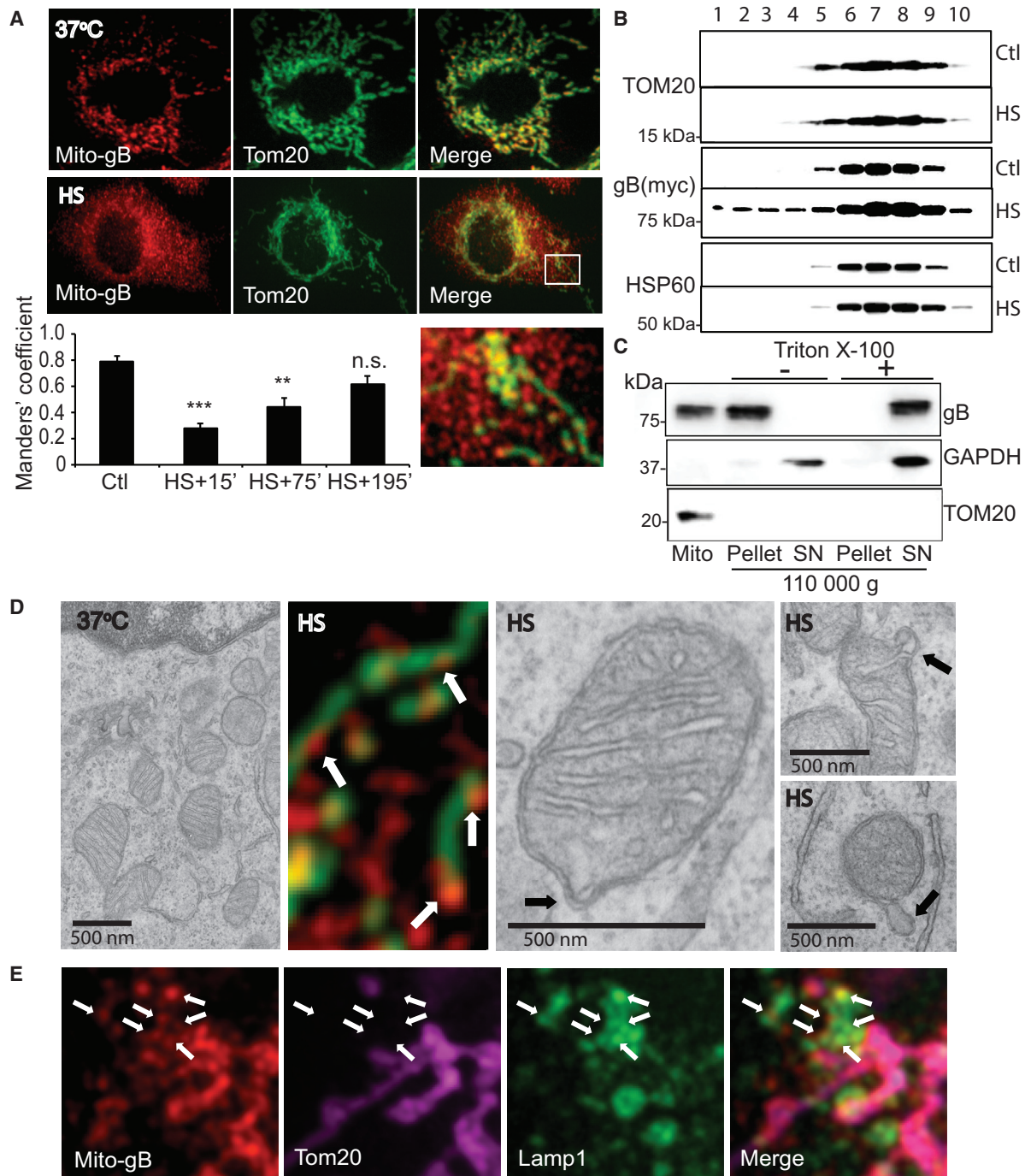


Figure 3. HS Induces Formation of MDVs

(A) Following HS, mito-gB dissociates from TOM20+ mitochondria and localizes to vesicular-like structures. Histogram shows the level of colocalization (Manders' coefficient) of the mito-gB and TOM20 signals after 45-min HS.

(B) Cells treated or not with HS were lysed, and the various organelles were separated on a continuous sucrose gradient before SDS-PAGE and western blotting. (C) Mitochondria were removed from a total cell lysate of HS-treated mito-gB RAW cells by immunoselection, followed by 15,000 × *g* centrifugation. The supernatant was then pelleted at 100,000 × *g* after treatment or not with Triton X-100, before SDS-PAGE and western blotting.

(D) Electron microscopy of RAW cells at 37°C or 15 min after the end of HS. Arrows show different stages of mitochondrial budding events, reminiscent of what is observed in high-magnification IF picture.

(E) IF shows mito-gB+ vesicular structures (arrows) close to Lamp1+ structures after HS. Data represent mean ± SD of one experiment, representative of at least three independent experiments. The *p* value is calculated using ANOVA analyses.

Snx9 downregulation had no effect on the presentation of NE-gB. Like Rab9, Snx9 was recruited to mitochondria during HS (Figure 5C). EM analysis showed an accumulation of small buds on the surface of mitochondria in both Rab9 and Snx9 KD cells (Figures 5D and 5E).

So far, our data indicate that PINK1 and Parkin selectively inhibit MitAP and that MDV formation requires the recruitment of Snx9 and Rab9 to mitochondria. The precise way by which PINK1 and/or Parkin regulates this pathway is unknown. Expression of GFP-Parkin in RAW macrophages, a condition shown to inhibit MitAP on HS (Figure 2D), inhibited the recruitment of Snx9 to mitochondria (Figure 5F). In the presence of GFP-Parkin, the cellular pool of Snx9 was degraded on HS, as shown by its decrease in total cell lysate (TCL). Interestingly, treatment with MG132 to inhibit the proteasome restored the pool of protein in the TCL and the recruitment of Snx9 to mitochondria during HS, suggesting that the ubiquitin ligase activity of Parkin plays a role in the degradation of Snx9. This proposal was supported by the finding that the expression of the two mutants of GFP-Parkin lacking E3 ligase activity (C431N and K211N) (McLelland et al., 2014) had no significant inhibitory effect on MitAP (Figure S4D) and did not affect the level of expression of Snx9 in the cell (TCL) or inhibit recruitment of Snx9 to mitochondria on HS (Figure S4E).

Presentation of Mitochondrial Antigens on MHC Class I Molecules Is Repressed by PINK1 and Parkin In Vitro and In Vivo

Next, we tested whether PINK1 and Parkin also repress the presentation of an endogenous mitochondrial antigen. For this we turned to PBC, a clinically relevant model of mitochondrial autoimmune disorder associated with the presentation of a peptide derived from the mitochondrial matrix protein 2-oxoglutarate dehydrogenase (OGDH) (Björkland et al., 1991). Using a CD8+ T cell hybridoma specifically recognizing an OGDH epitope loaded on MHC class I molecules (Kanaseki et al., 2006), we first observed that HS induced the formation of OGDH+ vesicles lacking Tom20 in RAW cells (Figure 6A). Second, presentation of OGDH was increased in ATG-5 KD RAW cells during HS and inhibited in cells silenced for either Rab9 or Snx9 (Figure 6B). As observed for mito-gB, induction of mitophagy with CCCP did not lead to the presentation of OGDH (data not shown). Third, the transient expression of GFP-Parkin in primary bone marrow-derived macrophages (BMDM) prompted the recruitment of GFP-Parkin to mitochondria (TOM20+) on HS, inhibiting the formation of OGDH+ vesicles (Figure 6C) and the presentation of this antigen on MHC I molecules (Figure 6D). Similar results were obtained for bone-marrow-derived dendritic cells (BMDC; data not shown). Fourth, we isolated BMDC from PINK1 knockout (KO) mice and showed an increase in the presentation of OGDH on HS treatment in vitro, compared to cells isolated from wild-type littermate animals (Figure 6E). Similar results were obtained with BMDM (data not shown). Together, these data demonstrate that an endogenous mitochondrial matrix enzyme, involved in the development of the autoimmune disease PBC, is presented on MHC class I molecules by a vesicular pathway consistent with the one described for the model antigen gB.

So far, we used a mild HS-mimicking fever (Hasday and Singh, 2000) to trigger MDV formation and MitAP. Inflammatory conditions and exposure to LPS, a mediator of inflammation, have been reported to reduce the level of Parkin in neurons and macrophages, leading to the proposal that chronic inflammatory conditions may phenocopy *parkin* loss-of-function mutations (Tran et al., 2011). This led us to examine whether LPS affects MitAP. As observed for HS, treatment of RAW cells with LPS and INF γ at 37°C (to mimic inflammatory conditions) induced the formation of mito-gB+/Tom20– vesicles (Figure 6F) and strongly stimulated gB presentation (Figure 6G). Additional HS treatment further enhanced MitAP. The stimulatory effect of LPS on MDVs and OGDH antigen presentation was also observed in BMDC and BMDM (data not shown). The pathway of mito-gB presentation induced by LPS displayed similar features as the one described for HS. It was inhibited in Snx9 and Rab9 KD cells, as well as in cells expressing GFP-Parkin, while an increase was observed in PINK1 KD cells (Figure 6H). These data show that PINK1 and Parkin also act to repress the presentation of gB during LPS treatment.

In addition to the role of PINK1 and Parkin in mitophagy, our data reveal that these proteins function in repressing MitAP in APCs (antigen-presenting cells) in vitro. Next, we addressed whether the proposed role for PINK1 and Parkin in limiting MitAP could be validated in vivo. To this end, we injected a single intravenous dose of LPS in 2- to 3-month-old PINK1 and Parkin KO and WT littermate control mice to determine whether this condition would induce OGDH presentation in dendritic cells (DC). 24 hr after LPS injection, we isolated CD11c+ DC by immunoselection using CD11c magnetic beads (Figure 6I) and co-cultivated them with the OGDH-specific CD8+ T cell hybridoma. OGDH presentation did not occur in DC from mice injected with PBS, while only a low level of presentation was detected in DC isolated from LPS-injected control animals. In contrast, injection of LPS in PINK1 and Parkin KO mice resulted in higher levels of OGDH presentation by DC (Figure 6J). These data confirm our in vitro findings, demonstrating a clear role for PINK1 in the inhibition of MitAP in vivo.

DISCUSSION

Our in vitro and in vivo data highlight a pathway for the presentation of mitochondrial antigens regulated by PINK1 and Parkin. Surprisingly, this pathway is not mediated by mitophagy, but rather is driven by the generation of MDVs. MDVs were originally described as MAPL-containing vesicles involved in the trafficking of selective mitochondrial cargo to peroxisomes (Neuspiel et al., 2008). Later, a second pathway was identified that carried oxidized cargo to the late endosome for degradation, a process stimulated on oxidative stress. The formation of these structures was Drp1 independent but required three of the PD-related proteins, PINK1, Parkin (for ROS-induced transport to late endosomes), and Vps35 (for delivery to peroxisomes) (Braschi et al., 2010; McLelland et al., 2014), highlighting the potential relevance of these structures in PD. Interestingly, Vps35 has been recently shown to play a role in MDV transport within dopaminergic neurons derived from PD patients (Tang et al., 2015; Wang et al., 2015). The mechanisms involved in the formation

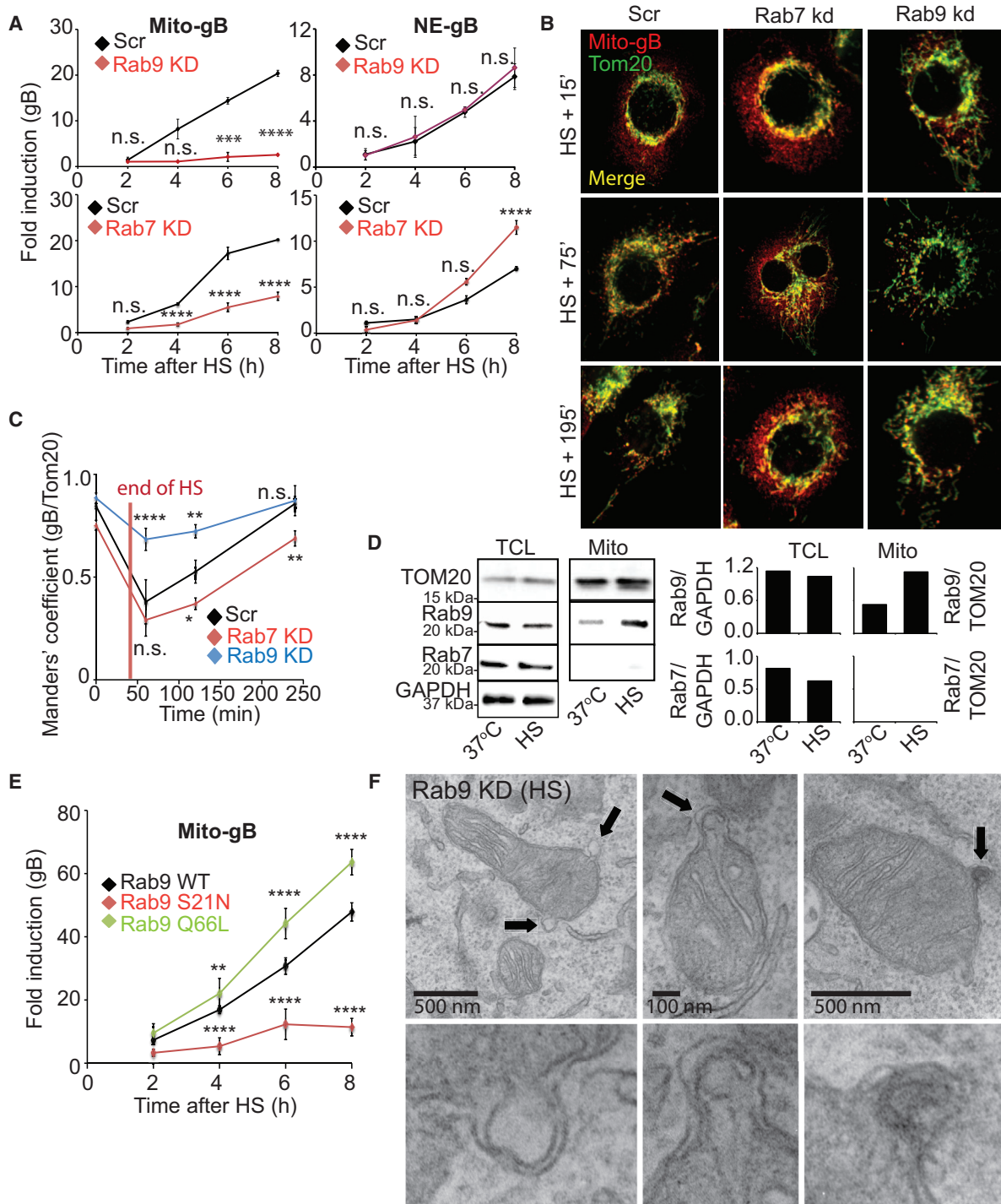


Figure 4. Mito-gB Vesicle Formation and MitAP Are Regulated by Rab9 and Rab7

(A) Downregulation of the expression of Rab9 and Rab7 inhibits mito-gB presentation, but not NE-gB (see also Figure S3).

(B) IF shows the dissociation and reassociation of mito-gB and TOM20 after HS. In the Rab7 KD cells the dissociation persists over time, while in the Rab9 KD cells mito-gB and Tom20 do not dissociate.

(C) Quantification of the kinetics of mito-gB and Tom20 colocalization in control cells (Scr), Rab7 KD, and Rab9 KD (Manders' coefficient).

(D) Rab9, but not Rab7, associates to mitochondria during HS.

(legend continued on next page)

of HS/LPS-induced MDVs differ from the two types of structures described above. Indeed, although they carry selected cargo and are generated in a Drp1-independent manner, the formation of HS/LPS-induced MDVs does not require PINK1 and Parkin. In fact, these two proteins actively inhibit their biogenesis. These results suggest that different pathways are engaged on ROS production and in response to HS/LPS. This was confirmed by showing that the PINK1/Parkin-dependent cargo PDH present in ROS-induced MDVs was not incorporated in HS-induced MDVs in COS7 cells. Concomitantly, OGDH present in HS/LPS-induced MDVs was not transferred to ROS-induced MDVs (Figure S5). Overall, these data highlight that mitochondria are highly dynamic organelles. Understanding the mechanisms of cargo incorporation and the structure/function of each class of MDVs will provide a better understanding of the complex mechanisms linking mitochondrial dynamic events with diseases.

We have found that two cytoplasmic proteins, Snx9 and Rab9, are required for HS/LPS-induced MDV formation and MitAP. Both of these proteins are involved in trafficking events occurring elsewhere in the cell. Snx9 is recruited to dynamin2 oligomers at the plasma membrane, where it coordinates actin polymerization and vesicle release (Yarar et al., 2007). Rab9 acts on late endosomes, where it regulates the formation of retrograde transport vesicles carrying Mannose-6-phosphate receptors to the trans-Golgi network (Carroll et al., 2001). Our data indicate that Snx9 and Rab9 accumulate on mitochondria on HS, demonstrating that proteins involved in MDV formation are actively recruited in response to stress. Our results also showed a direct correlation between the extent of MDV formation and MitAP. Conditions that stimulated MDV formation, such as HS and PINK1 KD, increased MitAP, while conditions resulting in a decrease of MDVs, such as Snx9 and Rab9 KD, decreased MitAP.

A mechanism that may have explained how PINK1 and Parkin inhibits MitAP is through a massive engagement of mitophagy, sequestering mitochondria within membrane structures and preventing the release of MDVs. This pathway was ruled out since no change in mitochondrial function or mass was observed after HS. Instead, the observations that gB- and OGDH-containing vesicles are rapidly released after HS (within the first 30 min), while MitAP occurs within 2 hr, suggests that PINK1 and Parkin rapidly repress MDV formation in response to HS/LPS stimulation. Our data suggest that Parkin controls MDV formation and MitAP by regulating the level of the cellular pool of Snx9 in a proteasome-dependent manner. In cells expressing GFP-Parkin, HS induces a rapid degradation of Snx9, preventing the recruitment of this protein to mitochondria. In this context, expression of a catalytically dead form of GFP-Parkin did not prevent MDV formation and MitAP. Whether Snx9 is a direct or indirect substrate of Parkin is not yet known, although the stability of Snx9 during HS is dependent on Parkin's enzymatic activity. Interest-

ingly, the association of Rab9 with mitochondria in heart tissue of OVE26 diabetic mice has been shown to occur in conditions in which mitophagy is inhibited and the level of PINK1 and Parkin expression is strongly decreased (Xu et al., 2013). These results suggest that Parkin-dependent mechanisms similar to those described here may also regulate the recruitment of cytoplasmic proteins to mitochondria in association with the cardiac dysfunction observed in these animals.

The finding that embryonic fibroblasts present OGDH after HS or LPS/IFN γ treatment (Figure S6A) suggests that cell types other than immune cells are able to perform MitAP and may thus be affected by PINK/Parkin mutations. After MDV formation, a second GTPase, Rab7, is required for MitAP, probably for fusion of the vesicles with late endosomes (as shown by the accumulation of vesicles in Rab7 KD cells). In late endosomes/lysosomes, mitochondrial antigens are processed by hydrolytic enzymes, as shown by the increase in presentation when cells are treated with protease inhibitors. Peptides are then likely to be translocated to the cytoplasm to be further processed by the proteasome, before loading on MHC I molecules in the ER, as suggested for cross-presentation (Houde et al., 2003). Expression of GFP-Parkin in RAW cells had no effect on the presentation of exogenous gB internalized by phagocytosis (inactivated HSV1 particles coated on latex beads) (English et al., 2009), ruling out the contribution of Parkin in regulating cross-presentation at common steps downstream of MDV transport to the late endosome (Figure S6B). Interesting aspects not been addressed in our study include the nature of the mitochondrial proteins, other than OGDH, processed and presented through the PINK1/Parkin-controlled MDV pathway, and the potential presentation of mitochondrial antigens on MHC class II molecules.

Inflammation and microglial activation in the brain of PD patients has led to the proposal that non-autonomous cell processes involving the immune system contribute to DA neuron degeneration (Dawson, 2008). Our data provide support for a non-cell-autonomous model in which autoimmune mechanisms mediated by cytotoxic T cell activity contribute to the destruction of DA neurons during PD. We argue that in addition to the role of PINK1/Parkin in mitochondrial quality control, the loss of their activity during PD would increase MitAP on cellular stress, such as inflammation. This is supported by our *in vivo* results in Parkin and PINK1 KO mice showing that a single injection of LPS is sufficient to induce MitAP in dendritic cells. Interestingly, LPS treatment was shown to induce subtle fine-motor deficits and selective loss of DA neurons in the substantia nigra of Parkin $-/-$ mice (Frank-Cannon et al., 2008). MitAP increase in APCs is likely to promote the establishment of peripheral mitochondrial antigen-specific T cell populations. In this context, neuroinflammation and microglia activation at a later age within PD patients would allow T cells to access the brain (Mosley et al., 2012). It is known that during infectious or inflammatory

(E) Mito-gB presentation was inhibited in cells expressing the S21N mutant of Rab9 (GDP bound) and stimulated when the Q66L mutant (GTP bound) was expressed.

(F) Electron microscopy of Rab9 KD cells 15 min after the end of HS. Arrows show the mitochondrial budding events. Data represent mean \pm SD of one experiment, representative of at least three independent experiments. The p value is calculated using two-way ANOVA analyses.

See also Figure S3.

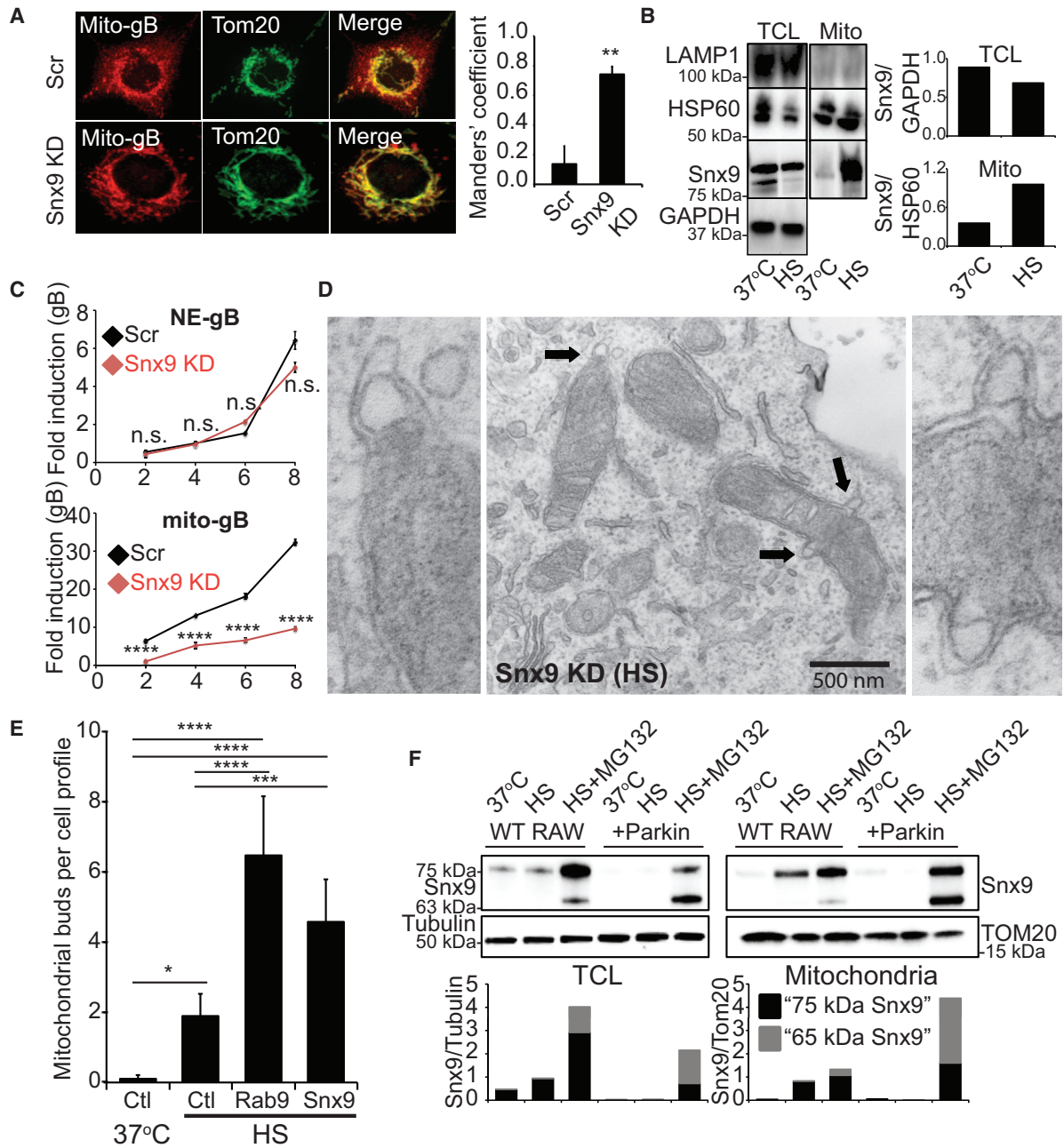


Figure 5. Mito-gB Vesicle Formation and MitAP Are Regulated by Snx9

(A) Mito-gB/Tom20 dissociation is strongly inhibited in Snx9 KD cells, as shown by the Manders' coefficient.
 (B) Snx9 is recruited to mitochondria during heat stress (HS).
 (C) Downregulation of the expression of Snx9 inhibits mito-gB presentation, but not NE-gB.
 (D) Electron microscopy of Snx9 KD cells 15 min after the end of HS. Arrows show mitochondrial budding events.
 (E) Mitochondrial buds were quantified by EM.
 (F) Expression of GFP-Parkin in RAW cells leads to the degradation of Snx9 in the TCL and the inhibition of Snx9 recruitment to mitochondria. See also Figure S4. Data represent mean \pm SD of one experiment, representative of at least three independent experiments. The p value is calculated using one-way (E) or two-way (C) ANOVA analyses.
 See also Figures S4 and S5.

conditions, peripheral immune cells access the CNS (Mosley et al., 2012). Blood-brain barrier dysfunctions have been reported in PD patients (Kortekaas et al., 2005; Pisani et al., 2012). Furthermore, a recent study has revealed the existence of a lymphatic system in the CNS that may facilitate the transport of immune cells (Louveau et al., 2015). Thus, mechanisms exist

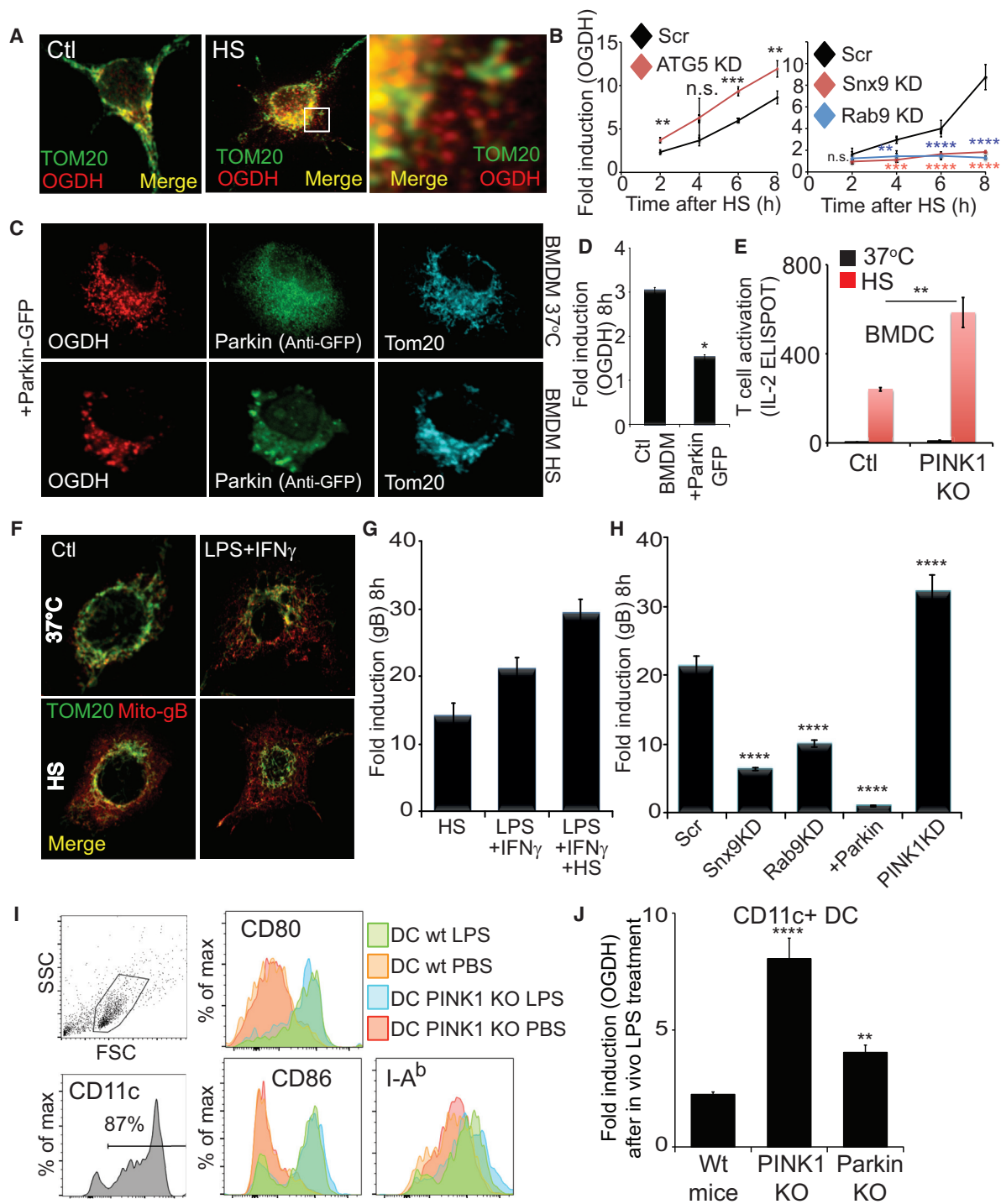


Figure 6. Presentation of OGDH Autoantigen on MHC Class I Is Driven by MDVs and Repressed by PINK1 and Parkin In Vitro and In Vivo

(A) OGDH and TOM20 dissociate after HS treatment in RAW cells.

(B) Downregulation of ATG5 stimulates OGDH presentation, while OGDH presentation is strongly inhibited in Snx9 and Rab9 KD cells.

(C) In primary bone-marrow-derived macrophages (BMDM) expressing GFP-Parkin the protein is recruited to mitochondria after HS, while OGDH stays with TOM20.

(D) OGDH presentation is inhibited in GFP-Parkin BMDM.

(E) Loss of Pink1 increases OGDH presentation in BMDC after HS.

(F) Pre-treatment of 24 hr with LPS+IFN γ before HS increases OGDH vesicle formation.

(legend continued on next page)

to allow T cell infiltration and direct access to DA neurons. Remarkably, DA neurons were shown to express MHC class I molecules at their surface in presence of activated microglia or other stressors linked to inflammation, becoming “visible” to the immune system (Cebrián et al., 2014). In this context, our data provide a mechanism whereby activation of MitAP in Parkin $-/-$ DA neurons would engage recognition by established mitochondria antigen-specific T cells, triggering a cytotoxic response that may ultimately lead to neuron cell death. Our work provides a new conceptual framework for future investigation into the contribution of MitAP within both DA neurons and immune cells in PD.

Lastly, the identification of the cell biological pathway responsible for MitAP also provides a mechanistic basis for the understanding of mitochondrial immune tolerance and related autoimmune disease. For example, our data demonstrate that the MDV-driven MitAP pathway is used to process and present OGDH on MHC class I molecules. OGDH is the source of the main autoantigen associated with the autoimmune disease PBC, where the contribution of both CD4+ and CD8+ T cell response has been demonstrated (Hirschfield and Gershwin, 2013). Autoimmunity is controlled by a fine balance between tolerance and the deleterious effect of an active immune response. This control is done in part by regulatory T cells (Tregs), which are major actors of peripheral tolerance. Adoptive transfer of Tregs has been shown to be a successful approach for the treatment of autoimmune cholangitis, a mouse model of PBC (Tanaka et al., 2014). Remarkably, Tregs also have been shown to exert a neuroprotective effect on the nigrostriatal system on adoptive transfer in MPTP-intoxicated mice, an animal model of PD (Olson and Gendelman, 2016; Reynolds et al., 2007). In PD patients, alteration in peripheral T lymphocyte populations, with an increase in CD8+ T cells and a decrease in Tregs, has been reported (Baba et al., 2005), supporting the potential involvement of autoimmune mechanisms in the progression of the disease. Overall, identification of PINK1 and Parkin as regulators of the immune system opens novel avenues for the development of effective treatments against PD.

EXPERIMENTAL PROCEDURES

Animals and Cells

BALB/c, C57BL/6, *Pink1* $-/-$, and *Parkin* $-/-$ mice were handled in strict accordance with good animal practice as defined by the Canadian Council on Animal Care and protocols approved by the Comité de déontologie animale of Université de Montréal. The RAW 264.7 macrophage cell line (ATCC), the H-2K^b RAW cell line (Bell et al., 2013), and COS7 cells (ATCC) were cultured in DMEM (10% [v/v] fetal calf serum [FCS], penicillin [100 units/ml], and streptomycin [100 μ g/ml]). The β -galactosidase-inducible HSV gB/K^b-restricted HSV-2.3.2E2 CD8+ T cell hybridoma (2E2) was kindly provided by F. Carbone (University of Melbourne). The OGDH/L^d and OGDH/K^b-restricted 2CZ CD8T⁺

cell hybridoma (Dutz et al., 1994; Udaka et al., 1993) was kindly provided by N. Shastri (University of California). Hybridomas were maintained in RPMI-1640 medium supplemented with 5% (v/v) FCS, glutamine (2 mM), penicillin (100 units/ml), and streptomycin (100 μ g/ml).

Immunofluorescence and Electron Microscopy

For IF microscopy, cells were fixed 15 min (37°C) with 5% paraformaldehyde (PFA). PFA was then quenched with 50 mM NH₄Cl/PBS for 10 min at room temperature (RT). Cells were permeabilized with 0.1% Triton X-100/PBS (v/v) for 10 min at RT and blocked with 5% FBS/PBS for 10 min. Cells were incubated with primary antibodies for 2 hr. After the several PBS washes, cells were incubated with secondary antibodies for 1 hr and observed with a Andor/Yokogawa spinning disk confocal system (CSU-X) attached to a Olympus IX81 inverted microscope and 100 \times or 60 \times objectives (na 1.4). For the quantification of gB+ MDVs, images stacks (0.4- μ m steps) were analyzed by ImageJ. Quantification was done on at least three experiments (10–15 cells/experiment). Mander's colocalization coefficient was measured using the JACoP plugin from ImageJ. For electron microscopy, cells were fixed in 2.5% (v/v) glutaraldehyde at 37°C for 45 min and embedded in Epon (Mecalab). Quantification of mitochondrial buds was performed on randomly selected cell profiles (in each experiment, at least 12 cell profiles per condition).

Biochemical Analyses

For density gradients, a post-nuclear supernatant from 10⁹ mito-gB RAW cells was loaded onto a 0.5–1.8 M sucrose gradient and centrifuged at 80,000 \times g for 18 hr. Fractions were collected and analyzed by western blotting. Mitochondria were purified using a mitochondria isolation kit (Miltenyi). In order to isolate vesicular structures containing mito-gB, the negative fraction after immunoselection was subjected to a second centrifugation (15,000 \times g, 15 min) to eliminate remaining mitochondria. The supernatant was collected and subjected to a third centrifugation (110,000 \times g, 45 min) to enrich smaller vesicular structures. As a control, 0.1% Triton X-100 (Sigma) was added to solubilize membrane-bound structures before the third centrifugation. Proteins were separated on 4%–15% pre-cast SDS-PAGE (BioRad) and processed for immunodetection by chemiluminescence (Amersham Biosciences).

MHC Class I Antigen Presentation Assay

2 \times 10⁵ APC were plated in triplicate and treated or not with a 45-min HS at 42°C and then returned to 37°C for a total time of 2, 4, 6, and 8 hr. Alternatively, cells were pre-incubated with LPS+IFN γ before HS. Cells were then fixed with 1% PFA for 10 min at RT and washed with RPMI, 10% FBS, and 0.1 M glycine. Finally 10⁵ 2E2 T cells were added for 16 hr, and β -galactosidase activity was measured at 595 nm after the addition of CPRG substrate. For OGDH antigen presentation using H2-L^d-expressing cells (Raw- and BALB/c-derived cells), 2CZ T cell hybridoma was used, and IL-2 secretion was measured using IL-2 ELISA (eBiosciences). As the 2CZ TCR affinity for the OGDH/K^b complex is much lower than the affinity for the OGDH/L^d complex (Dutz et al., 1994), we used an IL-2 ELISPOT assay (Mabtech) to measure OGDH antigen presentation by H2-K^b-expressing cells (C57BL/6 and *Pink1* $-/-$ derived cells).

In Vivo LPS Administration

6- to 12-week-old WT and *Pink1* and *Parkin* KO mice were injected intravenously (i.v.) with 10 μ g of liposaccharide (LPS). Mice were sacrificed 20 hr later, and CD11c+ DC were purified from spleen and lymph nodes using a pan-dendritic cells isolation kit (Miltenyi), followed by a positive selection using CD11c magnetic beads (Miltenyi). DC purity and activation level was assessed by fluorescence-activated cell sorting (FACS) (BD FACS Canto II). OGDH antigen

(G) LPS+IFN γ pre-treatment promotes OGDH antigen presentation.

(H) OGDH presentation is inhibited in the absence of Snx9 and Rab9, as well as when GFP-Parkin is expressed, while the absence of PINK1 promotes it.

(I) Splenic CD11c+ dendritic cells (DC) were isolated after i.v. administration of LPS to PINK1 and *Parkin* (data not shown) KO mice.

(J) LPS stimulation in vivo increases the presentation of OGDH in DC from PINK1 and *Parkin* KO mice. Data represent mean \pm SD of one experiment, representative of at least three independent experiments. The p value is calculated using one-way (H and J) and two-way (B) ANOVA analyses or the Student's t test (D and E).

See also Figure S6.

presentation by CD11c+ DC was measured using 2CZ hybridoma and IL-2 ELSIPOT.

Statistical Analyses

p values were calculated using Prism (GraphPad). Differences between the two groups were tested with a Student's t test, and the differences between three or more groups were tested by one-way or two-way ANOVA. Quantification of western blots was performed using ImageJ.

SUPPLEMENTAL INFORMATION

Supplemental Information includes Supplemental Experimental Procedures and six figures and can be found with this article online at <http://dx.doi.org/10.1016/j.cell.2016.05.039>.

AUTHOR CONTRIBUTIONS

D.M., A.S., A.B.P., A.L., C.R., M.C., A.F., J.J.B., L.-E.T., Y.B., and E.G. designed and performed the experiments and analyzed the data; D.M., H.M.M., and M.D. conceived and directed the work and prepared the manuscript with contributions from all authors; and all authors contributed to discussions.

ACKNOWLEDGMENTS

We thank F. Carbone, W. Heath (University of Melbourne), and N. Shastri (University of California) for the hybridomas. We thank J. Boulais, H. Soudeyns, and the Fondation Centre de cancérologie Charles-Bruneau for technical support. This work was supported by the Canadian Institutes for Health Research (MOP#133653, MOP#114869, MOP#5605, and MOP#133549), the Canada Research Chair, and the Japan Society for the Promotion of Science.

Received: December 21, 2015
Revised: March 22, 2016
Accepted: May 10, 2016
Published: June 23, 2016

REFERENCES

Baba, Y., Kuroiwa, A., Uitti, R.J., Wszolek, Z.K., and Yamada, T. (2005). Alterations of T-lymphocyte populations in Parkinson disease. *Parkinsonism Relat. Disord.* *11*, 493–498.

Baum, H. (1995). Mitochondrial antigens, molecular mimicry and autoimmune disease. *Biochim. Biophys. Acta* *1271*, 111–121.

Bell, C., English, L., Boulais, J., Chemali, M., Caron-Lizotte, O., Desjardins, M., and Thibault, P. (2013). Quantitative proteomics reveals the induction of mitophagy in tumor necrosis factor- α -activated (TNF α) macrophages. *Mol. Cell. Proteomics* *12*, 2394–2407.

Björkstrand, A., Mendel-Hartvig, I., Nelson, B.D., and Tötterman, T.H. (1991). Primary biliary cirrhosis (PBC): characterization of a monoclonal antibody (PBC-MoAb) having specificity identical with disease-associated autoantibodies. *Scand. J. Immunol.* *33*, 749–753.

Blum, J.S., Wearsch, P.A., and Cresswell, P. (2013). Pathways of antigen processing. *Annu. Rev. Immunol.* *31*, 443–473.

Braschi, E., Goyon, V., Zunino, R., Mohanty, A., Xu, L., and McBride, H.M. (2010). Vps35 mediates vesicle transport between the mitochondria and peroxisomes. *Curr. Biol.* *20*, 1310–1315.

Carroll, K.S., Hanna, J., Simon, I., Krise, J., Barbero, P., and Pfeffer, S.R. (2001). Role of Rab9 GTPase in facilitating receptor recruitment by TIP47. *Science* *292*, 1373–1376.

Cebrián, C., Zucca, F.A., Mauri, P., Steinbeck, J.A., Studer, L., Scherzer, C.R., Kanter, E., Budhu, S., Mandelbaum, J., Vonsattel, J.P., et al. (2014). MHC-I expression renders catecholaminergic neurons susceptible to T-cell-mediated degeneration. *Nat. Commun.* *5*, 3633.

Chavrier, P., Parton, R.G., Hauri, H.P., Simons, K., and Zerial, M. (1990). Localization of low molecular weight GTP binding proteins to exocytic and endocytic compartments. *Cell* *62*, 317–329.

Dawson, T.M. (2008). Non-autonomous cell death in Parkinson's disease. *Lancet Neurol.* *7*, 474–475.

Dong, B., Kakihara, K., Otani, T., Wada, H., and Hayashi, S. (2013). Rab9 and retromer regulate retrograde trafficking of luminal protein required for epithelial tube length control. *Nat. Commun.* *4*, 1358.

Dutz, J.P., Tsomides, T.J., Kageyama, S., Rasmussen, M.H., and Eisen, H.N. (1994). A cytotoxic T lymphocyte clone can recognize the same naturally occurring self peptide in association with a self and nonself class I MHC protein. *Mol. Immunol.* *31*, 967–975.

Eiyama, A., and Okamoto, K. (2015). PINK1/Parkin-mediated mitophagy in mammalian cells. *Curr. Opin. Cell Biol.* *33*, 95–101.

English, L., Chemali, M., Duron, J., Rondeau, C., Laplante, A., Gingras, D., Alexander, D., Leib, D., Norbury, C., Lippé, R., and Desjardins, M. (2009). Autophagy enhances the presentation of endogenous viral antigens on MHC class I molecules during HSV-1 infection. *Nat. Immunol.* *10*, 480–487.

Frank-Cannon, T.C., Tran, T., Ruhn, K.A., Martinez, T.N., Hong, J., Marvin, M., Hartley, M., Treviño, I., O'Brien, D.E., Casey, B., et al. (2008). Parkin deficiency increases vulnerability to inflammation-related nigral degeneration. *J. Neurosci.* *28*, 10825–10834.

Guermonez, P., Valladeau, J., Zitvogel, L., Théry, C., and Amigorena, S. (2002). Antigen presentation and T cell stimulation by dendritic cells. *Annu. Rev. Immunol.* *20*, 621–667.

Hasday, J.D., and Singh, I.S. (2000). Fever and the heat shock response: distinct, partially overlapping processes. *Cell Stress Chaperones* *5*, 471–480.

Heo, J.M., Ordureau, A., Paulo, J.A., Rinehart, J., and Harper, J.W. (2015). The PINK1-PARKIN mitochondrial ubiquitylation pathway drives a program of OPTN/NDP52 recruitment and TBK1 activation to promote mitophagy. *Mol. Cell* *60*, 7–20.

Hernandez, D.G., Reed, X., and Singleton, A.B. (2016). Genetics in Parkinson disease: Mendelian versus non-Mendelian inheritance. *J. Neurochem. Published online April 18, 2016.* <http://dx.doi.org/10.1111/jnc.13593>.

Hirschfield, G.M., and Gershwin, M.E. (2013). The immunobiology and pathophysiology of primary biliary cirrhosis. *Annu. Rev. Pathol.* *8*, 303–330.

Houde, M., Bertholet, S., Gagnon, E., Brunet, S., Goyette, G., Laplante, A., Princiotta, M.F., Thibault, P., Sacks, D., and Desjardins, M. (2003). Phagosomes are competent organelles for antigen cross-presentation. *Nature* *425*, 402–406.

Kanaseki, T., Blanchard, N., Hammer, G.E., Gonzalez, F., and Shastri, N. (2006). ERAAP synergizes with MHC class I molecules to make the final cut in the antigenic peptide precursors in the endoplasmic reticulum. *Immunity* *25*, 795–806.

Kannarkat, G.T., Boss, J.M., and Tansey, M.G. (2013). The role of innate and adaptive immunity in Parkinson's disease. *J. Parkinsons Dis.* *3*, 493–514.

Kortekaas, R., Leenders, K.L., van Oostrom, J.C., Vaalburg, W., Bart, J., Willemssen, A.T., and Hendrikse, N.H. (2005). Blood-brain barrier dysfunction in parkinsonian midbrain in vivo. *Ann. Neurol.* *57*, 176–179.

Kucera, A., Distefano, M.B., Berg-Larsen, A., Skjeldal, F., Repnik, U., Bakke, O., and Progida, C. (2015). Spatio-temporal resolution of Rab9 and Cl-MPR dynamics in the endocytic pathway. *Traffic* *17*, 211–229.

Lazarou, M., Sliter, D.A., Kane, L.A., Sarraf, S.A., Wang, C., Burman, J.L., Sidaris, D.P., Fogel, A.I., and Youle, R.J. (2015). The ubiquitin kinase PINK1 recruits autophagy receptors to induce mitophagy. *Nature* *524*, 309–314.

Liu, L., Feng, D., Chen, G., Chen, M., Zheng, Q., Song, P., Ma, Q., Zhu, C., Wang, R., Qi, W., et al. (2012). Mitochondrial outer-membrane protein FUNDC1 mediates hypoxia-induced mitophagy in mammalian cells. *Nat. Cell Biol.* *14*, 177–185.

Lombardi, D., Soldati, T., Riederer, M.A., Goda, Y., Zerial, M., and Pfeffer, S.R. (1993). Rab9 functions in transport between late endosomes and the trans Golgi network. *EMBO J.* *12*, 677–682.

- Louveau, A., Smirnov, I., Keyes, T.J., Eccles, J.D., Rouhani, S.J., Peske, J.D., Derecki, N.C., Castle, D., Mandell, J.W., Lee, K.S., et al. (2015). Structural and functional features of central nervous system lymphatic vessels. *Nature* 523, 337–341.
- Lundmark, R., and Carlsson, S.R. (2009). SNX9 - a prelude to vesicle release. *J. Cell Sci.* 122, 5–11.
- Martin, H.L., Santoro, M., Mustafa, S., Riedel, G., Forrester, J.V., and Teismann, P. (2016). Evidence for a role of adaptive immune response in the disease pathogenesis of the MPTP mouse model of Parkinson's disease. *Glia* 64, 386–395.
- McLelland, G.L., Soubannier, V., Chen, C.X., McBride, H.M., and Fon, E.A. (2014). Parkin and PINK1 function in a vesicular trafficking pathway regulating mitochondrial quality control. *EMBO J.* 33, 282–295.
- Mosley, R.L., Hutter-Saunders, J.A., Stone, D.K., and Gendelman, H.E. (2012). Inflammation and adaptive immunity in Parkinson's disease. *Cold Spring Harb. Perspect. Med.* 2, a009381.
- Mueller, S.N., Jones, C.M., Smith, C.M., Heath, W.R., and Carbone, F.R. (2002). Rapid cytotoxic T lymphocyte activation occurs in the draining lymph nodes after cutaneous herpes simplex virus infection as a result of early antigen presentation and not the presence of virus. *J. Exp. Med.* 195, 651–656.
- Narendra, D., Tanaka, A., Suen, D.F., and Youle, R.J. (2008). Parkin is recruited selectively to impaired mitochondria and promotes their autophagy. *J. Cell Biol.* 183, 795–803.
- Nedjic, J., Aichinger, M., Emmerich, J., Mizushima, N., and Klein, L. (2008). Autophagy in thymic epithelium shapes the T-cell repertoire and is essential for tolerance. *Nature* 455, 396–400.
- Neuspiel, M., Schauss, A.C., Braschi, E., Zunino, R., Rippstein, P., Rachubinski, R.A., Andrade-Navarro, M.A., and McBride, H.M. (2008). Cargo-selected transport from the mitochondria to peroxisomes is mediated by vesicular carriers. *Curr. Biol.* 18, 102–108.
- Nivon, M., Richet, E., Codogno, P., Arrigo, A.P., and Kretz-Remy, C. (2009). Autophagy activation by NFKappaB is essential for cell survival after heat shock. *Autophagy* 5, 766–783.
- Norton, M., Ng, A.C., Baird, S., Dumoulin, A., Shutt, T., Mah, N., Andrade-Navarro, M.A., McBride, H.M., and Screaton, R.A. (2014). ROMO1 is an essential redox-dependent regulator of mitochondrial dynamics. *Sci. Signal.* 7, ra10.
- Olson, K.E., and Gendelman, H.E. (2016). Immunomodulation as a neuroprotective and therapeutic strategy for Parkinson's disease. *Curr. Opin. Pharmacol.* 26, 87–95.
- Paludan, C., Schmid, D., Landthaler, M., Vockerodt, M., Kube, D., Tuschl, T., and Münz, C. (2005). Endogenous MHC class II processing of a viral nuclear antigen after autophagy. *Science* 307, 593–596.
- Pickrell, A.M., and Youle, R.J. (2015). The roles of PINK1, parkin, and mitochondrial fidelity in Parkinson's disease. *Neuron* 85, 257–273.
- Pisani, V., Stefani, A., Pierantozzi, M., Natoli, S., Stanzione, P., Franciotta, D., and Pisani, A. (2012). Increased blood-cerebrospinal fluid transfer of albumin in advanced Parkinson's disease. *J. Neuroinflammation* 9, 188.
- Reynolds, A.D., Banerjee, R., Liu, J., Gendelman, H.E., and Mosley, R.L. (2007). Neuroprotective activities of CD4+CD25+ regulatory T cells in an animal model of Parkinson's disease. *J. Leukoc. Biol.* 82, 1083–1094.
- Soubannier, V., McLelland, G.L., Zunino, R., Braschi, E., Rippstein, P., Fon, E.A., and McBride, H.M. (2012). A vesicular transport pathway shuttles cargo from mitochondria to lysosomes. *Curr. Biol.* 22, 135–141.
- Sugiura, A., McLelland, G.L., Fon, E.A., and McBride, H.M. (2014). A new pathway for mitochondrial quality control: mitochondrial-derived vesicles. *EMBO J.* 33, 2142–2156.
- Tanaka, H., Zhang, W., Yang, G.X., Ando, Y., Tomiyama, T., Tsuneyama, K., Leung, P., Coppel, R.L., Ansari, A.A., Lian, Z.X., et al. (2014). Successful immunotherapy of autoimmune cholangitis by adoptive transfer of forkhead box protein 3(+) regulatory T cells. *Clin. Exp. Immunol.* 178, 253–261.
- Tang, F.L., Liu, W., Hu, J.X., Erion, J.R., Ye, J., Mei, L., and Xiong, W.C. (2015). VPS35 Deficiency or Mutation Causes Dopaminergic Neuronal Loss by Impairing Mitochondrial Fusion and Function. *Cell Rep.* 12, 1631–1643.
- Tran, T.A., Nguyen, A.D., Chang, J., Goldberg, M.S., Lee, J.K., and Tansey, M.G. (2011). Lipopolysaccharide and tumor necrosis factor regulate Parkin expression via nuclear factor-kappa B. *PLoS ONE* 6, e23660.
- Trost, M., English, L., Lemieux, S., Courcelles, M., Desjardins, M., and Thibault, P. (2009). The phagosomal proteome in interferon-gamma-activated macrophages. *Immunity* 30, 143–154.
- Udaka, K., Tsomides, T.J., Walden, P., Fukusen, N., and Eisen, H.N. (1993). A ubiquitous protein is the source of naturally occurring peptides that are recognized by a CD8+ T-cell clone. *Proc. Natl. Acad. Sci. USA* 90, 11272–11276.
- Vanlandingham, P.A., and Ceresa, B.P. (2009). Rab7 regulates late endocytic trafficking downstream of multivesicular body biogenesis and cargo sequestration. *J. Biol. Chem.* 284, 12110–12124.
- Wang, W., Wang, X., Fujioka, H., Hoppel, C., Whone, A.L., Caldwell, M.A., Cullen, P.J., Liu, J., and Zhu, X. (2015). Parkinson's disease-associated mutant VPS35 causes mitochondrial dysfunction by recycling DLP1 complexes. *Nat. Med.* 22, 54–63.
- Xu, X., Kobayashi, S., Chen, K., Timm, D., Volden, P., Huang, Y., Gulick, J., Yue, Z., Robbins, J., Epstein, P.N., and Liang, Q. (2013). Diminished autophagy limits cardiac injury in mouse models of type 1 diabetes. *J. Biol. Chem.* 288, 18077–18092.
- Yarar, D., Waterman-Storer, C.M., and Schmid, S.L. (2007). SNX9 couples actin assembly to phosphoinositide signals and is required for membrane remodeling during endocytosis. *Dev. Cell* 13, 43–56.

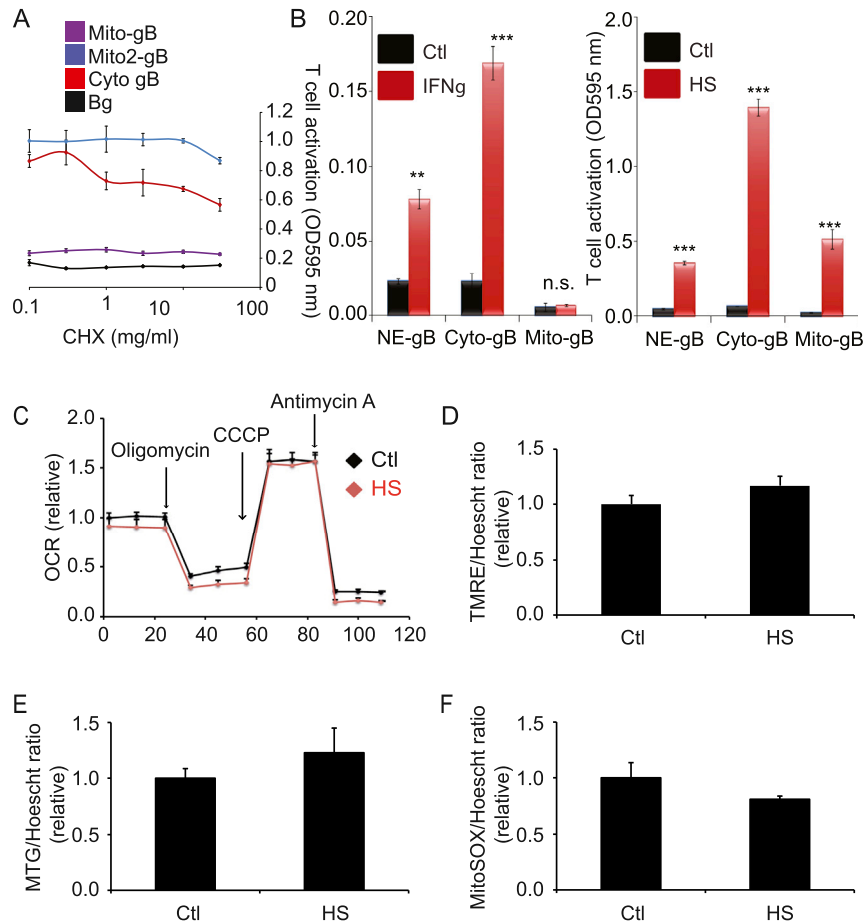


Figure S1. Mitochondrial Functions Are Preserved in RAW Macrophages Following Heat Shock, Related to Figure 1

(A) Raw data showing the effect of CHX in mito-gB, mito2-gB and cyto-gB MHC-I presentation. Data represent mean \pm SD of one experiment representative of at least 3 independent experiments.

(B) Raw data of MG132 and Bafilomycin on the presentation of gB following IFN γ - or HS-treatment. Data represent mean \pm SD of one experiment representative of at least 3 independent experiments. p value is calculated using one-way ANOVA analyses.

(C–F) Mitochondrial oxygen consumption rate (OCR) (C), membrane potential (D), mitochondrial content (E), and mitochondrial superoxide (F) production measured 4 hr after exposure of RAW macrophages to heat shock (15 min at 42°C). OCR was measured on a Seahorse XF24 extracellular flux analyzer, and normalized against basal respiration in non-heat shock exposed cells. Following measurement of basal OCR, Oligomycin, CCCP and antimycin-A were sequentially added to assess ATP-linked, maximal, and non-mitochondrial respiration, respectively. Membrane potential, mitochondrial content, and mitochondrial superoxide production were measured in parallel on a fluorescence plate reader using the potentiometric probe TMRE (10 nM), the membrane potential-independent dye Mitotracker green (1 μ M), and the mitochondria-targeted superoxide sensitive probe MitoSOX (25 μ M). In all experiments an equivalent number of cells (250 000) were plated in each well. However, raw fluorescence for each probe was normalized against Hoescht fluorescence to control for any variation in cell number post seeding. For TMRE, and Mitotracker green labeling, negative controls were run in parallel by incubating cells in presence of the mitochondrial uncoupler CCCP (1 μ M). For mitoSOX labeling, positive controls were performed by incubating cells in presence of the complex III blocker antimycin-A (100 μ M). The data reported represent Mean \pm SEM for two distinct cell cultures. All measurements were performed in triplicates.

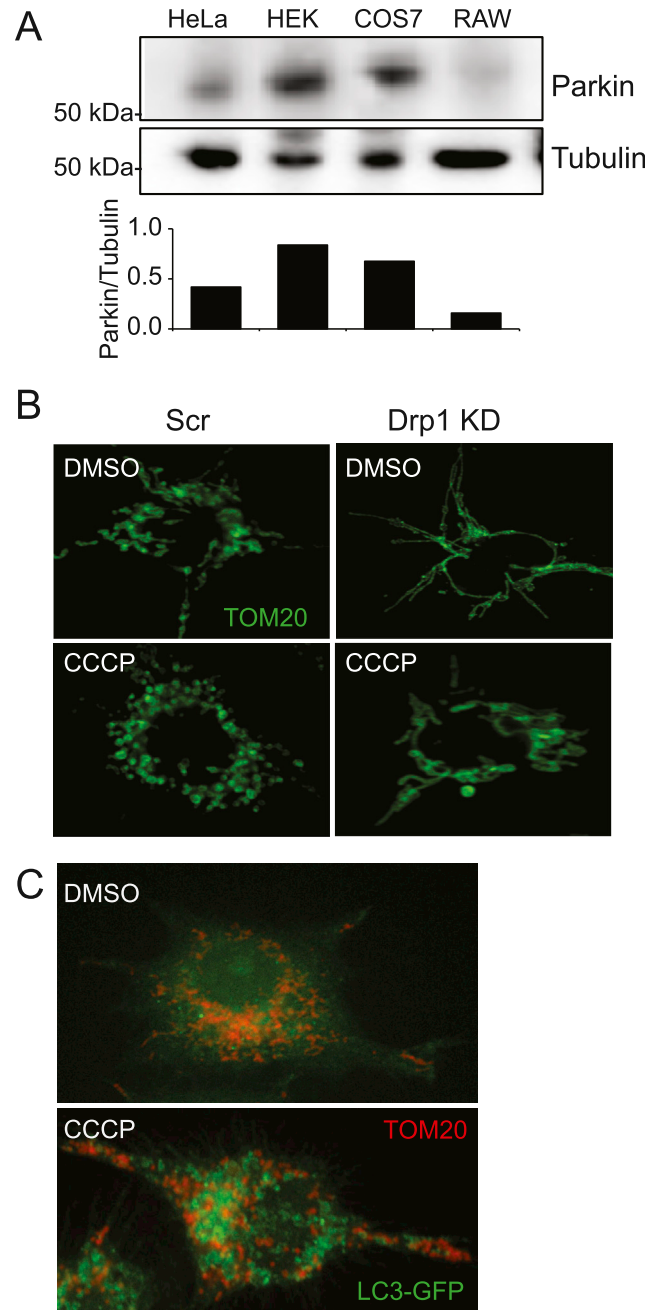


Figure S2. Mitophagy Is Not Responsible for MitAP, Related to Figure 2

(A) Western blot shows low Parkin expression level in RAW cells compared to HEK and COS7 cells, while the expression in HELA is also low. Histogram shows densitometric quantification of Parkin.

(B) IF shows the inhibition of mitochondria fragmentation in Drp1 KD RAW cells after CCCP treatment.

(C) IF shows LC3-GFP increase in expression and recruitment to mitochondria after CCCP treatment.

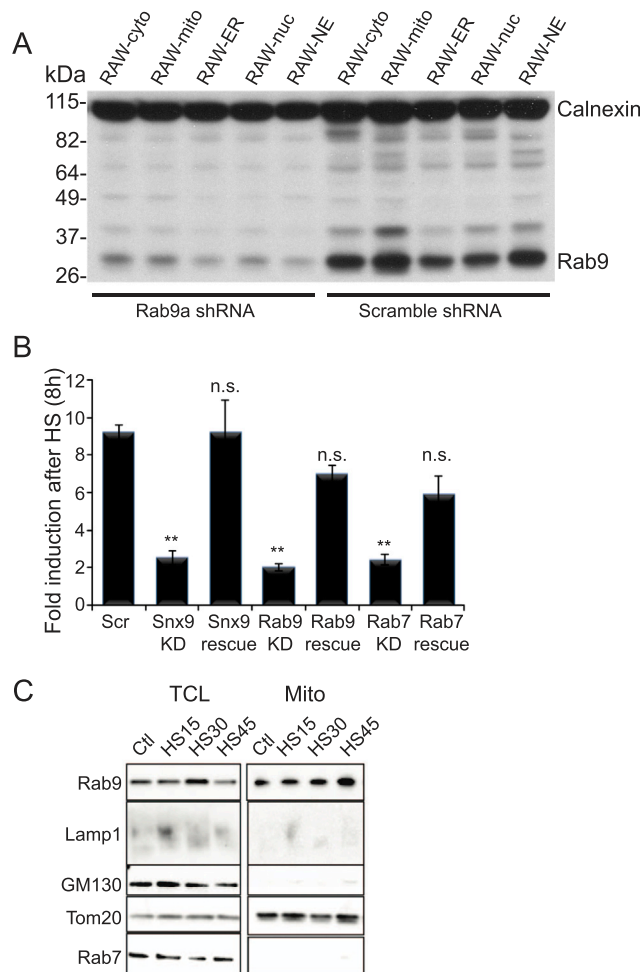


Figure S3. KD Efficiency and Mitochondria Purification, Related to Figure 4

(A) Western blot shows Rab9 KD efficiency in the various RAW cells used in this study. Please note that the RAW-ER and RAW-nuc forms of gB were not used in this study.

(B) Mito-gB presentation after HS is rescued in Snx9, Rab9 and Rab7 KD cells after expressing siRNA resistant Snx9, Rab9 and Rab7 proteins respectively.

(C) Absence of contaminants by Golgi (GM130) and endosomal compartments (Lamp1, Rab7) in the mitochondrial fraction isolated by immunoselection was assessed using western blotting.

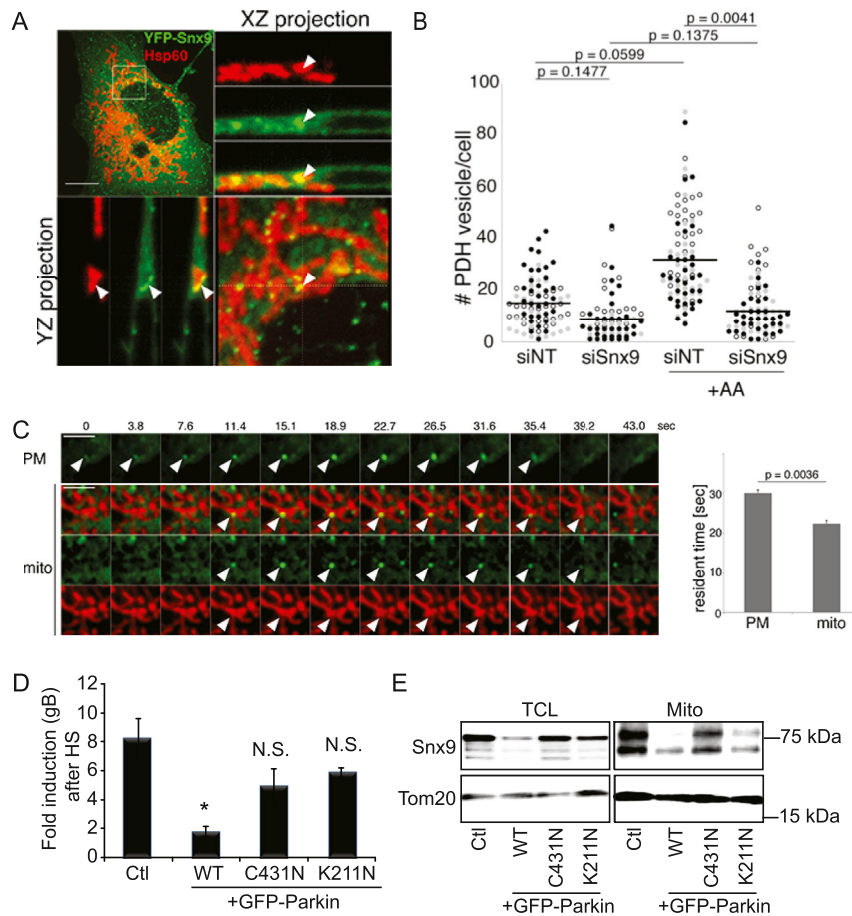


Figure S4. Mito-gB Vesicle Formation and MitAP Are Regulated by Snx9 and Parkin, Related to Figure 5

(A) 3D reconstruction image of COS7 cell expressing YFP-Snx9. Arrowheads indicate Snx9 recruited to mitochondria labeled with anti-Hsp60 antibodies.

(B) COS7 cells were transfected with NT (Non Targeted) or Snx9-targeted siRNA then treated with Antimycin A (AA) for MDV induction. MDVs were analyzed by co-staining with anti-Tom20 and -PDH antibodies. Dot plots represent the number of each MDV per cell, taken from 3 independent experiments. p value was calculated by Student's t test.

(C) Snx9 is recruited to sites of MDV formation along mitochondria. COS7 cells were transfected with YFP-Snx9 and mitochondria were stained with MitoTracker prior to live confocal imaging. Graph represents residence times of Snx9 at the mitochondria and plasma membrane. The error bars represent SEM. p value was calculated by Student's t test.

(D) Expression of functional Parkin tagged to GFP in RAW cells inhibited the presentation of gB during HS, while the expression of two inactive Parkin mutants had no effect.

(E) WB analyses indicate that the E3 ligase activity of Parkin is required to inhibit the recruitment of Snx9 to mitochondria.

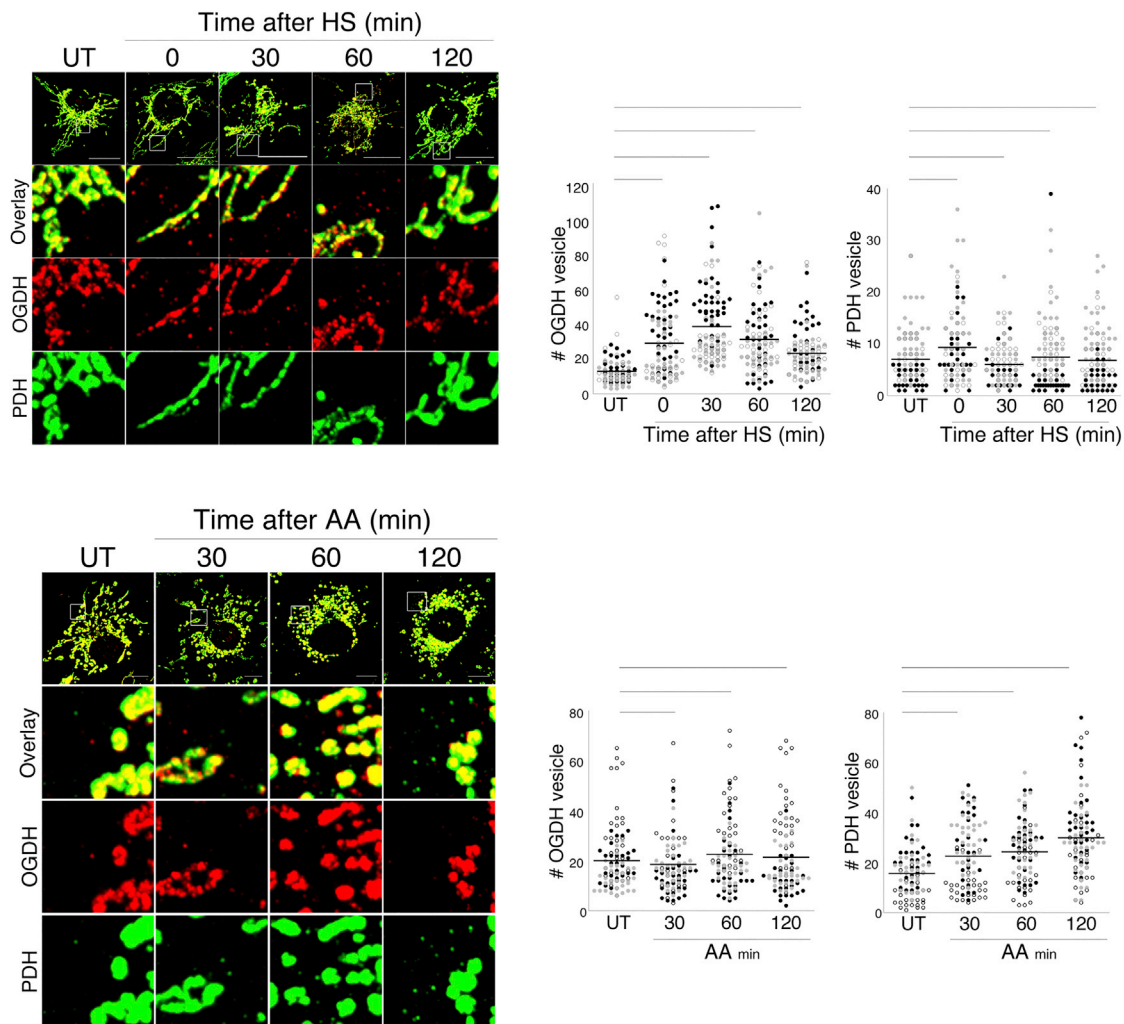


Figure S5. HS- and ROS-Induced Vesicles Select Distinct Cargoes, Related to Figure 5

Upper left panel displays IF showing that OGDH dissociates from mitochondria after HS while PDH maintains a typical mitochondria staining in COS7 cells. The upper right panel shows values for the number of OGDH+ or PDH+ vesicles counted per cell in 3 independent HS experiments (black, grey, and white). Bars represent the mean. p value was calculated by Student's t test. Lower left panel displays IF showing that after AA treatment, PDH dissociates from the mitochondria, while OGDH is retained in mitochondria. The lower right panel shows values for the number of OGDH+ or PDH+ vesicles counted per cell in 3 independent AA treatment experiments (black, grey, and white). Bars represent the mean. p value was calculated by Student's t test.

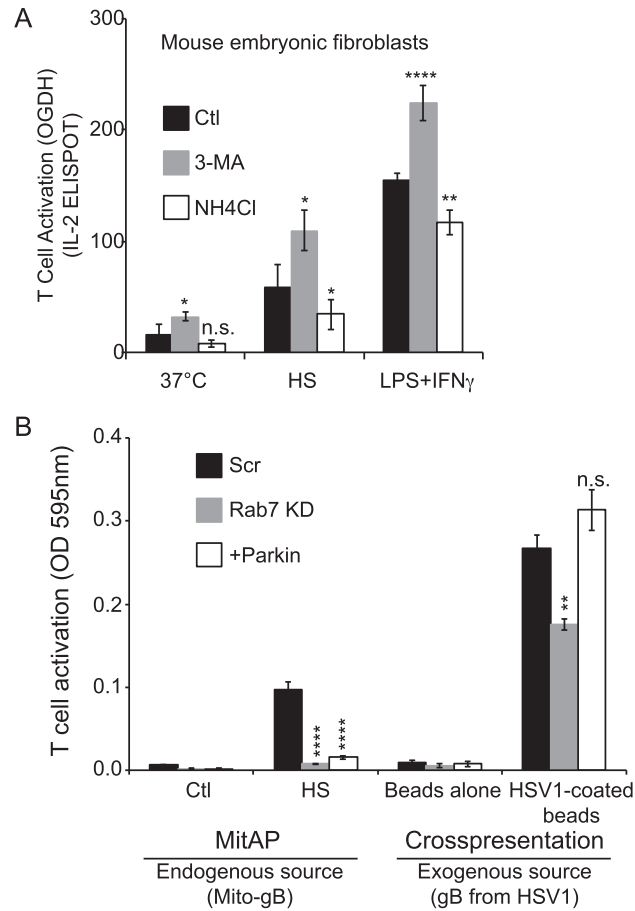


Figure S6. MitAP in Non-immune Cells and Role of Cross-presentation in mito-gB Presentation, Related to Figure 6

(A) Histogram shows OGDH presentation in MEF cells after HS or LPS+IFN γ treatment in the presence of 3-MA or NH4Cl.

(B) Histogram shows that mito-gB presentation is inhibited after HS in Rab7 KD RAW cells or in RAW cells expressing GFP-Parkin. In contrast, cross-presentation of exogenous gB internalized by phagocytosis is not affected by the presence of GFP-Parkin. Data represent mean \pm SD of one experiment representative of at least 3 independent experiments. p value was calculated using one-way ANOVA analyses.

Cell, Volume 166

Supplemental Information

Parkinson's Disease-Related Proteins

PINK1 and Parkin Repress

Mitochondrial Antigen Presentation

Diana Matheoud, Ayumu Sugiura, Angélique Bellemare-Pelletier, Annie Laplante, Christiane Rondeau, Magali Chemali, Ali Fazel, John J. Bergeron, Louis-Eric Trudeau, Yan Burelle, Etienne Gagnon, Heidi M. McBride, and Michel Desjardins

SUPPLEMENTAL EXPERIMENTAL PROCEDURES

Design of shRNA and Knockdown Strategy

Specific shRNAs targeting ATG5, Rab9, Rab7, Snx9, Pink1, Drp1 and nontargeting scramble (Scr) controls were designed based on the sequences from the Sigma-Aldrich MISSION- RNA website. Annealed forward and reverse hairpin oligonucleotides were cloned into a modified pLKO.1-TRC1.5 vector where the puromycin-resistance gene was replaced with mAmetrine. Lentiviral particles were made by cotransfecting HEK293T cells with the shRNA-containing pLKO-mAM vector along with pMD2-VSVG, pMDLg/pRRE, and pRSV-REV. Viral supernatants were used for transduction and cells were sorted according to mAmetrine fluorescence. Validation of the knockdown was done by real-time qPCR and western blot analyses. For rescue experiments dog RAB7 and RAB9 as well as human SNX9 gene sequences were PCR-amplified from plasmids containing the genes and cloned directly in the respective shRNA-containing pLKO-mAM vectors. The inserts were cloned upstream of mAmetrine and driven by the pLKO pgk promoter. Lentiviral particles were produced and transduced as described above.

Reagents and Antibodies

Antibodies against gB (ab6506), Tom20 (ab115746), PDH (ab110330), GM130 (ab52649), Mitofusin 1 (ab57602) and GFP (ab5450) were purchased from Abcam. The antibody against Snx9 (1E4) was purchased from GeneTex. The antibody against OGDH (HPA020347) was purchased from SIGMA. The antibody against GAPDH was from Millipore (MAB374). Antibodies against Tom20 (sc-11415) and Parkin (sc-32282) were from Santa Cruz, and anti-Lamp1 from Developmental Studies Hybridoma Bank University of Iowa. Anti-Rab9 (5118S), anti-Rab7 (9367S), anti-Hsp60 (12165S), anti-Tubulin (2148S) and anti-LC3b (2775S) were purchased from Cell Signaling. Secondary antibodies (anti-rabbit AF488 A-11008, anti-mouse AF488 A-11001, anti-rabbit AF568 A-11011, anti-mouse AF568 A-11004, AF647 anti-rat A-21242) were from Invitrogen. CD11c-PE (HL3), I-A^b-FITC (AF6-120.1), CD80-PerCP Cy5.5 (16-10A1) and CD86 APC (GL1) were purchased from BD Biosciences.

3-Methyladenine (1 mM), Bafilomycin A1 (0.5 μ M), NH₄Cl (10 mM), Cocktail of Protease Inhibitor (P1860, 1:1000) and CCCP (Carbonyl cyanide 3-chlorophenylhydrazone, 20 μ M) were from Sigma. MG132 (2 μ M) was from Calbiochem. LPS (200 ng/ml) was from Invivogen; IFN γ (200 U/ml) was from PeproTech.

Plasmids

The full length sequence coding for HSV-1 gB (gB₁₋₂₇₁₅) was cloned from purified HSV-1 DNA (strain F). The sequence was truncated using the primers GTAAC TAGTCTCCGACTTCCCCCG and GTAGATATCCTTGATCTCGTGGCGGGTGA containing, respectively, the restriction sites SpeI and EcoRV. gB₃₀₋₂₀₉₄ lacked both the signal peptide and the transmembrane domain of the viral gB (the coded protein is predicted to stay in the cytoplasm).

The full length gB and gB₃₀₋₂₀₉₄ were cloned in a pIRES2-EGFP constructs to generate the full-gB and the cyto-gB expression vectors. Alternatively, gB₃₀₋₂₀₉₄ was cloned in pIRES2-EGFP- Mito kindly provided by Claude Perreault (Université de Montréal). The resulting vectors contained the backbone of pIRES2-EGFP including, in the multiple cloning sites, a cassette containing the mitochondrial matrix-targeting sequence (from human cytochrome *c* oxidase, MSVLTPLLLRGLTGSARRLPVPRAKIHSL) followed by gB₃₀₋₆₉₄, generating the mito-gB expressing vector. RAW-K^b cells were stably transfected with these three different vectors using the TransIT-LT1 reagent (according to the manufacture's procedure, Mirus) and selected with G418 at 0.5 mg/ml.

pEGFP-Parkin vector was provided by Michael Shlossmacher (Ottawa Hospital). A eGFP-Rab9 WT expressing lentiviral vector was created by first cloning EGFP into pHAGE-CMV- fullEF1a-IRES-ZsGreen (PlasmID) replacing the IRES-ZsGreen. Rab9 was then amplified from murine primary cells cDNA and cloned after EGFP and linked by a short flexible linker. This construct was used as a template to create the lentiviral vectors expressing the EGFP-Q66L or EGFP-S21N mutants (Diaz et al., 1997) by overlap PCR. Lentiviral particles were then generated in HEK293T cells and used to transduce Raw macrophage cells to create stable cell lines. pEGFP-Snx9 kindly gifted from Dr. Rohan D. Teasdale (The University of Queensland) was used as template to subclone full length and fragments of Snx9 into pEYFP-C1 vector (Clontech) using primers GGAATTCTATGGCCACCAAGGCTCGG and GACGTCGACTACATCACTGGAAAGCG. Cells were

transfected using the TransIT-LT1 reagent and cells selected according to the GFP fluorescence.

Crosspresentation

For gB-HSV1 latex bead coupling, 1.9 μm NH_2 -Latex Beads (LBs) (Estapor) were washed in PBS and precoated with Helix pomatia lectin (EY Laboratories) at 1 mg/ml overnight with agitation. Then, LBs were washed again with PBS and incubated overnight with purified HSV-1 (strain F) at 4°C with agitation, and finally, HSV-1 particles were inactivated by UV irradiation. Cells were then incubated with beads for 6h, fixed and tested for MHC-I presentation.

SUPPLEMENTAL REFERENCES

Diaz, E., Schimmoller, F., and Pfeffer, S.R. (1997). A novel Rab9 effector required for endosome-to-TGN transport. *J Cell Biol* 138, 283-290.